Theses and Dissertations

12-2014

Design of a High Performance Silicon Carbide CMOS Operational Amplifier

Shaila Amin Bhuyan
University of Arkansas, Fayetteville

Follow this and additional works at: http://scholarworks.uark.edu/etd

Part of the Electronic Devices and Semiconductor Manufacturing Commons, and the VLSI and Circuits, Embedded and Hardware Systems Commons

Design of a High Performance Silicon Carbide CMOS Operational Amplifier

Design of a High Performance Silicon Carbide CMOS Operational Amplifier

A thesis submitted in partial fulfillment
of the requirements for the degree of
Master of Science in Electrical Engineering

by

Shaila Amin Bhuyan
University of Dhaka
Bachelor of Science in Applied Physics, Electronics and Communication Engineering, 2012

December 2014
University of Arkansas

This thesis is approved for recommendation to the Graduate Council

_____
Dr. H. Alan Mantooth
Thesis Director

_____
Dr. Simon Ang
Committee Member

_____
Dr. A. Matthew Francis
Committee Member

ABSTRACT

This thesis presents the design, simulation, layout and test results of a silicon carbide (SiC) CMOS two-stage operational amplifier (op amp) with NMOS input stage. The circuit has been designed to provide a stable open-loop voltage gain (60 dB), unity-gain bandwidth (around 5 MHz) and maintain a high CMRR and PSRR within a useful input common mode range over process corners and a wide temperature range (25 °C – 300 °C). Between the two stages a Miller compensation topology is placed to improve the phase margin (around 45^0). Due to the comparatively high threshold voltage values of transistors in SiC, the power supply is maintained at 15 V. There is a maximum of 21% variation in DC gain from 25 ^{0}C to 275 ^{0}C and the unity-gain bandwidth and slew rate improves with higher temperature. The major application area of this op amp is in high temperature environments where silicon (Si) integrated circuits (IC) fail to perform. In addition, the design of a second version of the operational amplifier is covered, which aims to provide more functionality and improved performance.

ACKNOWLEDGEMENTS

DEDICATION

This thesis is dedicated to my husband, Fahad Hossain, who has always been my biggest supporter, my sisters Fahima Amin Bhuyan & Saima Amin Bhuyan for always believing in me and most importantly to my parents Dr. Aminul Haque Bhuyan and Farida Begum for their unconditional love and confidence in me.

TABLE OF CONTENTS

LIST OF FIGURES

LIST OF TABLES

CHAPTER 1

INTRODUCTION

An operational amplifier (op amp) is the primary building block in analog and mixed-signal integrated circuits (ICs) and systems. It has a vast range of applications including DC bias generation, data conversion, sensor circuits, high-speed amplification and filtering. The op amp has several electrical characteristics such as, offset, gain-bandwidth (GB), slew rate, input common mode range (ICMR), as well as frequency response characteristics such as phase margin, that need to be considered during the design process [1]. At high temperatures (greater than 225 ^{o}C) the performance parameters show promising results when silicon (Si) and silicon-on-insulator (SOI) based devices are limited by leakage to operation at 125 ^{o}C and 225 ^{o}C, respectively [2]. The main objective of this thesis is the design of a SiC Complementary Metal Oxide Semiconductor (CMOS) op amp that is capable of reliable operation at high temperatures (25 °C to more than 300 °C) where Si and SOI ICs cannot perform well.

This thesis presents a two-stage op amp designed to drive a small purely capacitive load using an analog/mixed-signal SiC CMOS Process Design Kit (PDK) developed by Ozark IC and the University of Arkansas students who were a part of NSF-BIC project [3]. A three-stage op amp has also been designed in the next design cycle to provide more functionality and improved performance. The future implementation of the op amp circuit is used in, but not limited to, protection circuitry of a high temperature SiC gate driver.

1.1   Overview of Operational Amplifier

Op amps are amplifiers that can be described as high gain differential amplifiers. They are differential input, single output amplifiers that usually operate in conjunction with an external feedback system. Their open loop gain is maintained at a designed high value, so that when used in negative feedback closed loop system the transfer function does not have to depend on the gain [4]. The ideal op amp is defined as a general purpose op amp which has infinite differential-voltage gain, infinite bandwidth, infinite input impedance, zero bias currents and zero output impedance [5].
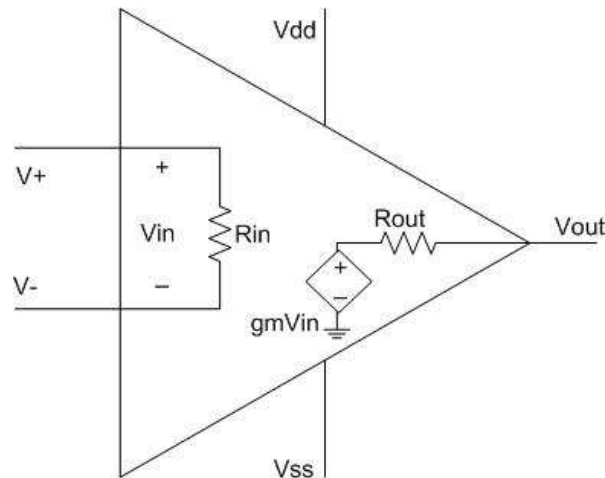
Fig. 1.1.1. Operational amplifier equivalent circuit [5].

In the Fig. 1.1.1 the op amp equivalent circuit has been illustrated. The practical op amp exhibits few non-ideal linear characteristics as shown in the Fig. 1.1.2 [6] Table 1.1 represents these non-ideal characteristics.

TABLE 1.1 NON IDEAL LINEAR CHARACTERISTICS OF OP AMP

Parameter	Symbol	Unit
Differential input resistance	Rid	Ω
Differential input capacitance	Cid	fF
Common mode input resistance	Ricm	Ω
Input offset voltage	Vos	mV
Input bias currents	Ib1 & Ib2	nA
Common mode rejection ratio	CMRR	---
Voltage noise spectral density	en2	mean sq volts/Hz
Current noise spectral density	in2	mean sq amps/Hz
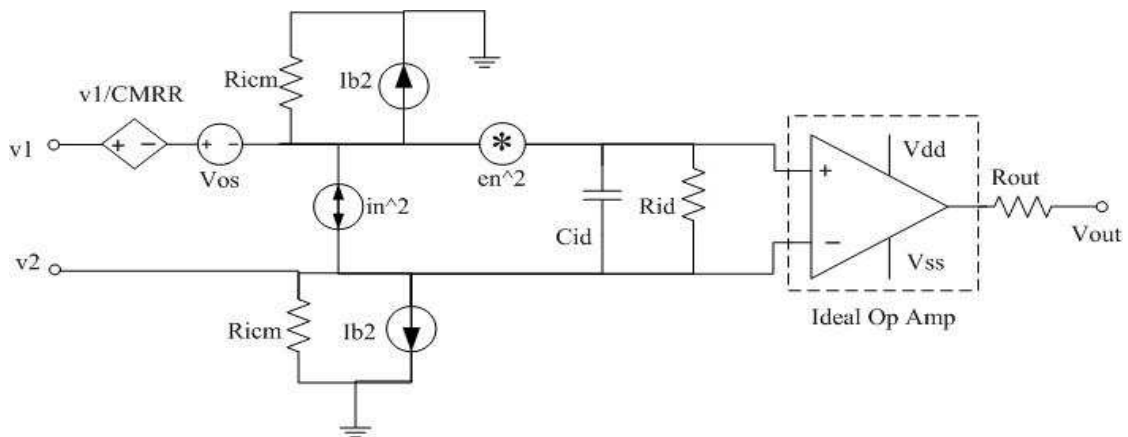
Fig. 1.1.2. Non-ideal linear characteristics of op amp [6].

3

One of the advantages of a CMOS op amp is that in negative feedback the common mode characteristics can be ignored. Also, the values of R_{id}, R_{icm}, I_{b1} and I_{b2} can be ignored easily due to the high input resistance of the MOS devices [6]. The output voltage V_{out} can be expressed as a sum of the differential portion, $A_v(s)$, and the common-mode portion, $A_c(s)$ as shown in below,

$$V_{out}(s) = A_v(s)[v_1(s) - v_2(s)] \pm A_c(s) \left(\frac{v_1(s) + v_2(s)}{2} \right) \tag{1.1}$$

$$A_v(s) = \frac{A_v(0)}{\left(\frac{s}{p_1} - 1\right)\left(\frac{s}{p_2} - 1\right)\left(\frac{s}{p_3} - 1\right)\dots} \tag{1.2}$$

Here p_1, p_2, p_3, ... are the poles of the differential-frequency response.

The unity-gain bandwidth (*GB*) characteristics can be defined as the frequency where the frequency response curve crosses the 0 dB line. In other words if the dominant pole is p_1 and the DC gain is $A_v(0)$ then,

$$GB = A_v(0).|p_1| \tag{1.3}$$

Other characteristics of interest are the Power Supply Rejection Ratio (*PSRR*) and the Common Mode Rejection Ratio (*CMRR*), which are defined in equation (1.4) and equation (1.5) respectively,

$$PSRR = \frac{\Delta V_{dd}}{\Delta V_{out}} A_v(s) = \frac{\frac{V_{out}}{V_{in}} (V_{dd} = 0)}{\frac{V_{out}}{V_{dd}} (V_{in} = 0)} \tag{1.4}$$

$$CMRR = 20 \log \left| \frac{A_v(0)}{A_c(0)} \right| \tag{1.5}$$

The input common mode range (*ICMR*) is the allowable voltage range of the input common-mode signal and the slew rate (*SR*) is the rate of change of the output voltage (measured in

volts/s) due to an abrupt change in the input voltage. *ICMR and SR* are large signal characteristics.

1.2   Applications

The op amp has vast applications in signal processing and mixed-signal systems, where it is commonly used in the interface between the differential input stage and the analog to digital converters (ADC). Due to the available high temperature functionality of SiC CMOS op amps, they are a good match to use for signal conditioning and sensor circuitry of SiC-based power switching devices. A few of the major applications of op amps and operational transconductance amplifiers (OTAs) are active filters, data converters, sensors, signal conditioning and signal amplifiers [7]. Some of the applications of op amps are described briefly below:

1.2.1   *2nd order Active Low Pass Filter*

Op amps and OTAs are used as an active element in signal processing and filter design as they provide high frequency operation with less sensitivity and simpler circuit topology [8]. The schematics of a 2nd order active low pass filter are shown in Fig. 1.2.1 below. The circuit has low quality factor sensitivity and low natural frequency when compared with passive filters.
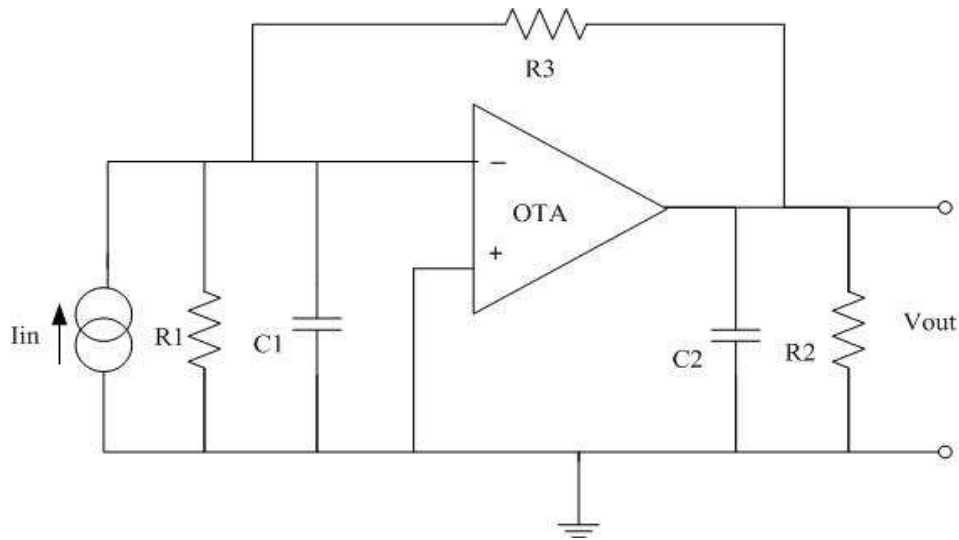
Fig. 1.2.1. 2nd order active low pass filter [8].

1.2.2 *Digital to Analog Data Converters*

Op amps have applications in data converters, both digital to analog converters (DAC) and analog to digital converters (ADC). The primary advantage of using an op amp in DAC is that the output load can be any arbitrary value rather than a fixed known capacitive value [9]. Fig. 1.2.2 shows the schematics of a traditional current mode R-2R ladder DAC. The required phase margin of the op amp is set very high (90°) to have a fast settling time. The output swing can be increased by increasing the open-loop gain or speed or by adding another op amp.
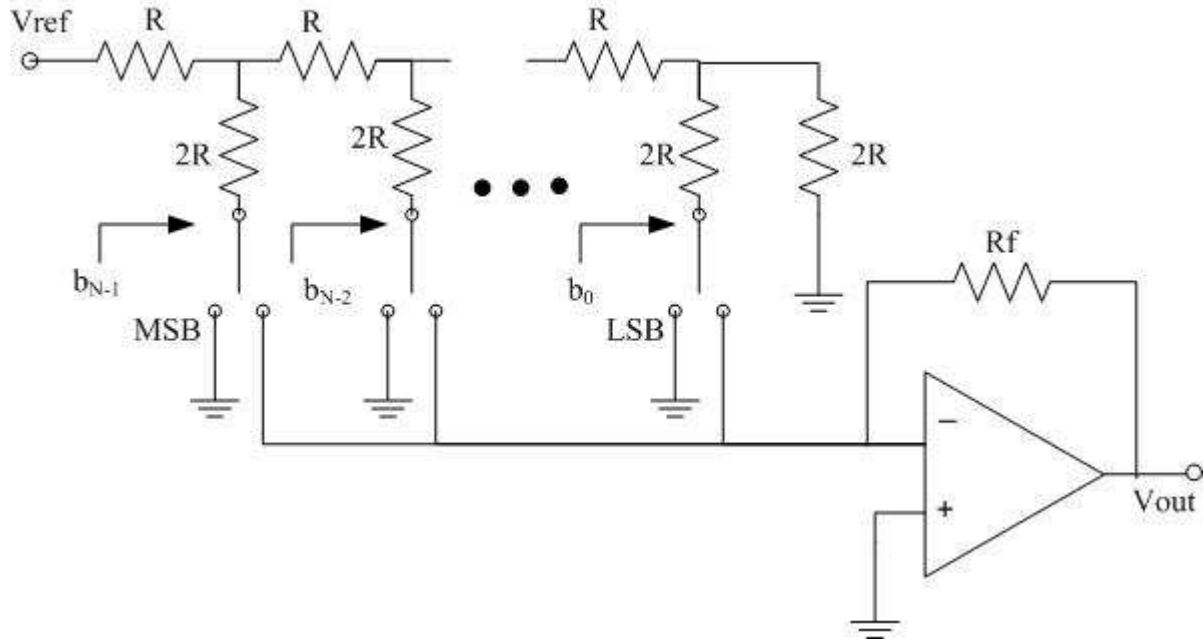
Fig. 1.2.2. Current mode R-2R DAC [9].

1.2.3 High-Side Current Sensing Circuit

The principle of the high side current sensor for a power switch converter is that it detects the current through the measured path and converts it to a proportional voltage. Fig. 1.2.3 shows the schematics of a current sensor with single op amp difference amplifier. The op amp detects and amplifies the voltage through the sensing resistor (R_{SEN}) and produces the measurable output (*Vout*) [10]. High-side current sensing is required to monitor the accidental short circuit current detection for the protection circuitry in power conversion systems. One of the major advantages of using op amps in this type of circuitry is low cost, low power dissipation and high common mode rejection ratio.

7
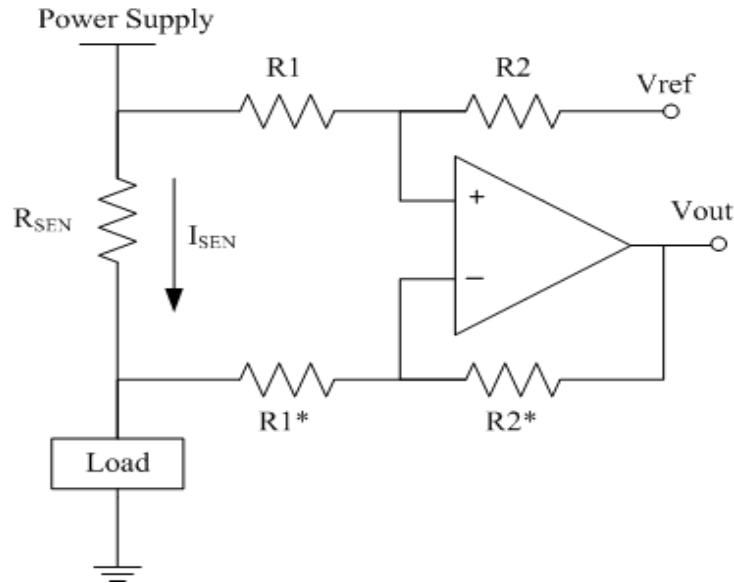
Fig. 1.2.3. Current sensor with single op amp difference amplifier [10].

1.3   Silicon Carbide CMOS Technology

SiC is a wide bandgap semiconductor material that can operate in temperatures up to 450 °C [11]. A SiC CMOS integrated circuit (IC) technology has applications in automotive, aerospace and deep well drilling as well as in SiC power electronics. The high temperature sensors and signal processing circuits that can be built using a SiC CMOS op amp will be beneficial for these systems [11]. The 15-V SiC CMOS technology used for this work is presented here. The process parameters are given below:

- Operating temperature up to 400 °C

- 1.2 µm minimum feature size, single metal process

- 40 nm electrical oxide equivalent thickness

- 15 V gate to source operating voltage
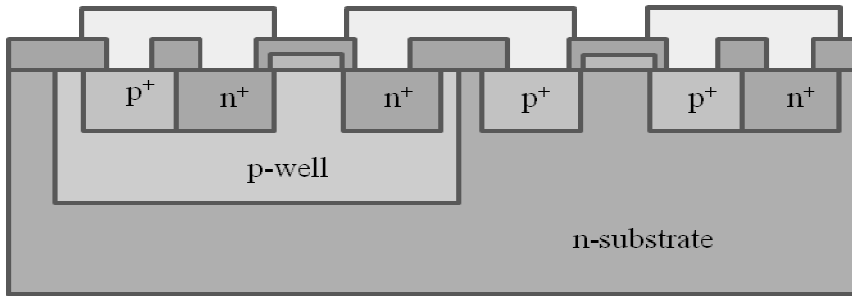
Fig. 1.3.1. SiC CMOS process architecture.

Fig. 1.3.1 shows the SiC CMOS process architecture. The substrate is an n+ 4H SiC Si-faced wafer with a doped epi-layer. The process includes epitaxial deposition and ion implantation to form the p- and n- regions. Further ion implantation process took place to create p+ and n+ source/drain regions and threshold voltage adjustment. All implants are annealed together. Afterwards the gate dielectrics, thick field oxide and the polysilicon gate electrodes are developed. The p+ and n+ regions will have ohmic metal contacts build followed by the deposition of patterned refractory metal interconnect. The last step in the process technology is to form a passivation layer.

1.4 Thesis Organization

The organization of the thesis is as follows: Chapter 2 covers the different topologies that have been considered for the design process. In Chapter 3 the actual design process for the selected topology along with the specifications, equations and hand calculation has been presented. Chapter 4 covers the simulation of the DC, AC and transient analysis in different temperature and corners. This is followed by Chapter 5 which presents the actual layout of the designed op amp. Chapter 6 covers the packaging information, the test setups and practical results at different temperatures. Finally, Chapter 7 covers the conclusion and the recommendations for future work.

9

CHAPTER 2

OPERATIONAL AMPLIFIER TOPOLOGIES

The operational amplifier can be implemented using a variety of topologies depending on the application requirements, process parameters, frequency mode, required characteristic performance and the degree of complexity available. Based on each specific design application, different topologies have been developed. Special considerations have been taken to study topologies that are most reliable and have a low level of complexity since the process technology in use is still in a developing stage. Research on previously developed topologies has been analyzed in this chapter.

2.1 Two-Stage Miller Compensated CMOS Op Amp

One of the basic structures of an op amp is the two stage CMOS op amp. In this structure the first stage is the differential transconductance stage which provides most of the op amp gain, followed by the second stage, which is a common source stage, that mainly provides a large output swing as [4] shown in the Fig. 2.1.1.
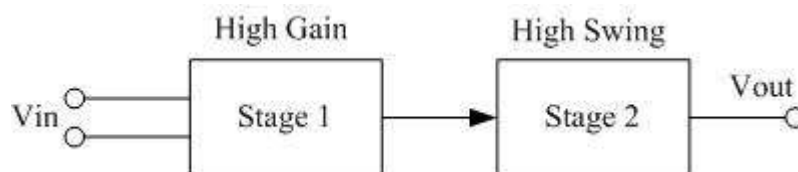
Fig. 2.1.1. Block diagram of a two-stage op amp [4].

Here the differential to single-ended conversion takes place in the first stage and the output stage is not followed by any buffer stage (the output resistance is very high). The transistors in both amplifier stages are properly biased to operate in the saturation region by using a current mirror or a beta multiplier as the biasing circuit. The circuit needs a compensation strategy due to the stability issue that arises when used in a closed-loop negative feedback system. The compensation can be accomplished by using Miller techniques where a capacitor is placed across the second amplifier stage. This creates a feedback path through the capacitor and employs the pole splitting technique [12]. This technique moves the poles of the open loop frequency response further away from the origin of the complex frequency plane, with the exception of the dominant pole which will move closer to the origin. This will also create a right-half plane (RHP) zero which can be positioned by placing a nulling resistor in series with the capacitor. The overall schematic of the topology is presented in Fig. 2.1.2 below. The main advantages of the two-stage system are its robustness and the simplicity. They are the most widely used topology and heavily reliable with a new process technology [13].
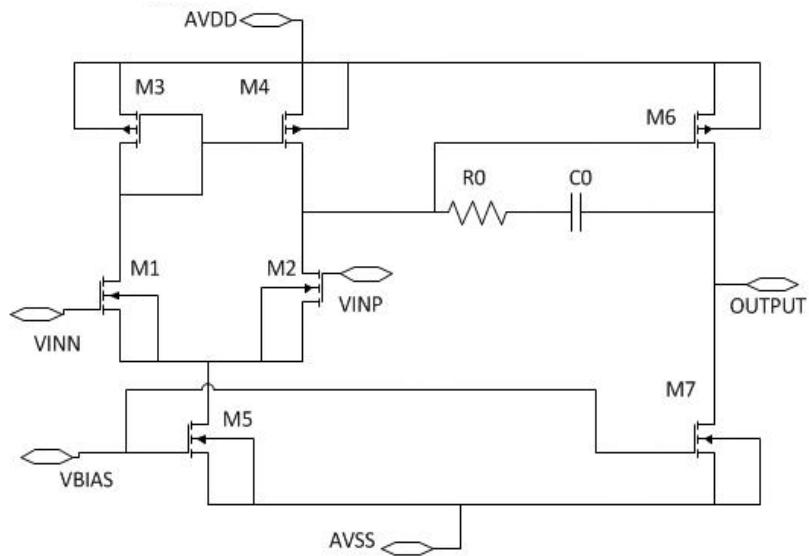
Fig. 2.1.2. Unbuffered, two-stage CMOS op amp schematic.

11

2.2 Three-Stage Nested Miller Compensation CMOS Op Amp

The three-stage op amp is used in analog and mixed-signal circuits to achieve higher DC gain and low power consumption from the supply voltage [9]. The block diagram of the three-stage nested Miller compensated (NMC) op amp is shown in Fig. 2.2.1. The circuit has three amplifier stages for high DC gain and two capacitors for stability. The capacitors create the frequency compensation needed for stability [14].
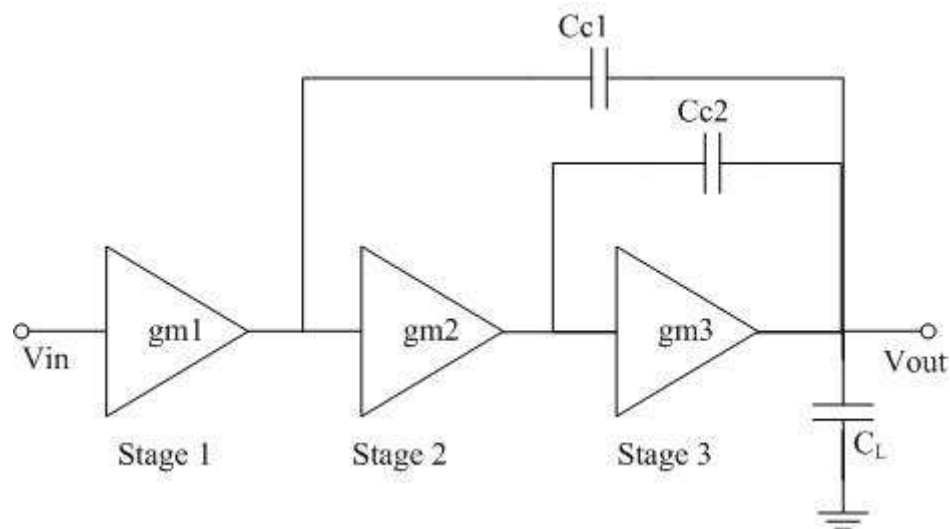
Fig. 2.2.1. Three-stage NMC op amp block diagram [14].

The first two stages of the Fig. 2.2.1 can be assumed to be a cascade of two differential amplifiers followed by the third stage which can be a common source amplifier. The Fig. 2.2.2 shows an actual topology of a three-stage op amp. Here the capacitors are placed in such a way so that the feedback current through C_{c1} combines with the feedback current through C_{c2} and flows towards the first stage. So, the compensation techniques implemented in Fig. 2.2.2 are an indirect nested Miller compensation method [9]. The main advantage of this topology is that, by

using two differential amplifier stages, all of the transistors in the topology are biased with known currents.
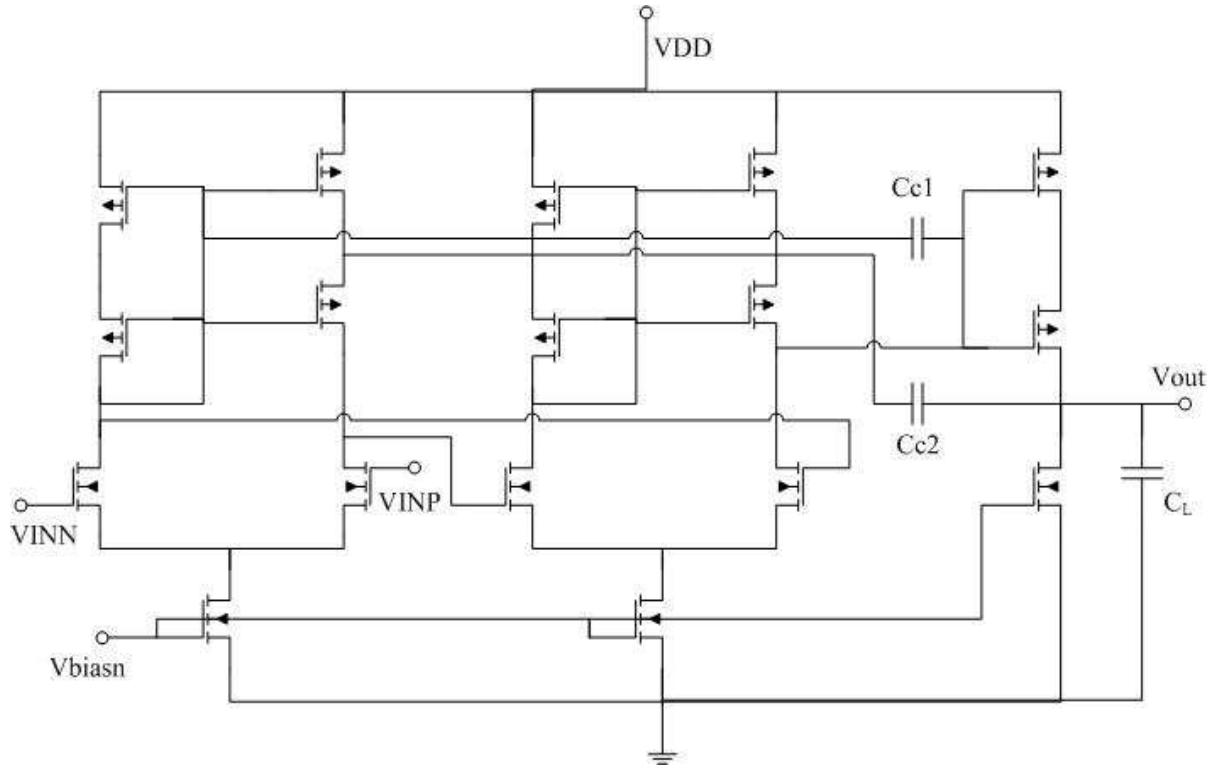
Fig. 2.2.2. Three-stage op amp schematic [9].

CHAPTER 3

CMOS OPERATIONAL AMPLIFIER DESIGN

3.1 Design Procedure

The design flow of the CMOS operational amplifier includes defining the requirements of the amplifier, defining the process design kit, stating the targeted inputs and outputs, hand calculations, simulations, layout, fine tuning the circuit based on parasitics, fabrication and testing. For a successful design the designer should have a clear idea about the needs of the system and each step of the design procedure. It is the designer's responsibility to successfully execute all the steps to ready the design for fabrication.

The general steps for integrated circuit design according to [6] are presented below:

1. Definition of the function and performance capability of the design: CMOS operational amplifier design for high temperature performance.

2. Synthesis or implementation: Silicon Carbide CMOS process.

3. Simulation or modeling: Estimate the device parameters based on hand calculations. Run simulation under different corners and temperature range to confirm the defined characteristic specifications.

4. Geometrical description: Complete the layout using proper toolchain and perform the design rule check.

5. Simulation including the geometrical parasitics: Consider the parasitic effects introduced by the layout and re-simulate the amplifier to reconfirm the performance characteristics.

6. Fabrication: When confident with the results of 1-5 above, the circuit is submitted for fabrication.

7. Testing & Verification: Develop the test and verification plan. Test the amplifier in real world scenario and compare with simulation results.

At this point, the next design process begins by adding the amplifier improvements identified from test data analysis obtained from the first fabrication run.

3.2 Design Specifications

TABLE 3.1 OPERATIONAL AMPLIFIER DESIGN SPECIFICATIONS

Parameter	Symbol	Value	Unit
Supply Voltage	AVDD	15	V
Temperature Range	T_A	25 – 300	^{o}C
Gain	A_V	60	dB
Gain Bandwidth	GB	5	MHz
Phase Margin	P.M.	45	Degree
Slew Rate	SR	10	V/μs
Input Common Mode Range	ICMR	5 – 14	V
Output Voltage Swing	ΔVout	2 – 14	V
Load Capacitance	C_L	10	pF

The key design specifications of the CMOS SiC op amp are given in Table 3.1. The primary motivation of the design process was to have a functional operational amplifier in a CMOS SiC process. For this reason, the degree of complexity has been kept at minimum and the design specifications were targeted rationally. Due to the high threshold voltages of the MOSFETs in the SiC process the supply voltage is higher than usual (15 V). The capacitive load has been specified as 10 pF so that the amplifier would be able to drive the load capacitances of testing equipment, i.e. oscilloscope probes. The circuit must work properly over a wide range of temperature while maintaining a high *CMRR* and *PSRR* within an acceptable input common-mode range.

3.3   Circuit Design

The CMOS SiC operational amplifier has two stages. One differential input stage followed by a common-source amplifier output stage. An additional compensation circuit is added between these two stages for better stability and improved phase margin. The biasing of the circuit is accomplished by using an external voltage source to reduce the circuit complexity and to have a better control over the circuit quiescent point. The circuit does not include any buffer stage and thus the load has been kept as a small capacitive value. The complete circuit schematic is shown in Fig. 3.1.
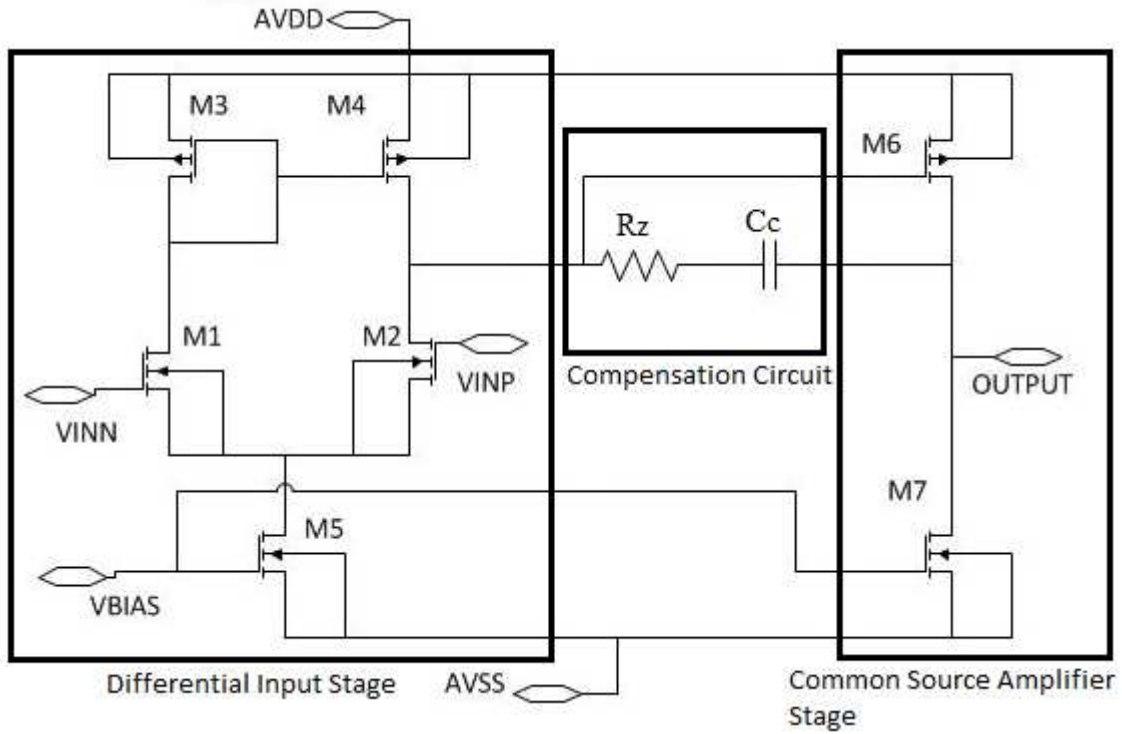
Fig. 3.3.1. Two-stage operational amplifier schematic.
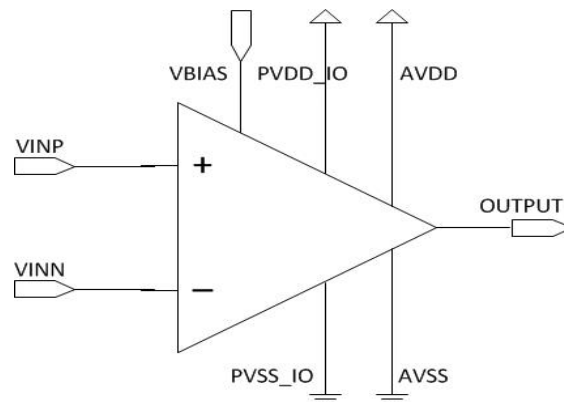
Fig. 3.3.2. The two-stage op amp symbol.

Fig. 3.3.2 represents the input and output ports of the op amp. The circuit has a total of 8 pins: AVDD and AVSS for power supplies, VINP and VINN for positive and negative inputs respectively, VBIAS for voltage biasing, PVDD_IO and PVSS_IO for power supplies to padframe and OUTPUT for the output.

17

3.3.1 Compensation Circuit

The compensation circuit is placed between the input and output of the second stage. It consists of a compensation capacitor (Miller capacitor) in series with a resistor (nulling resistor) as shown in Fig. 3.3.3. The purpose of the Miller capacitor is to introduce Miller feedback to obtain a single time-constant, dominant pole amplifier and the purpose of the nulling resistor is to position the right-half plane zero of the system created by the Miller feedback.
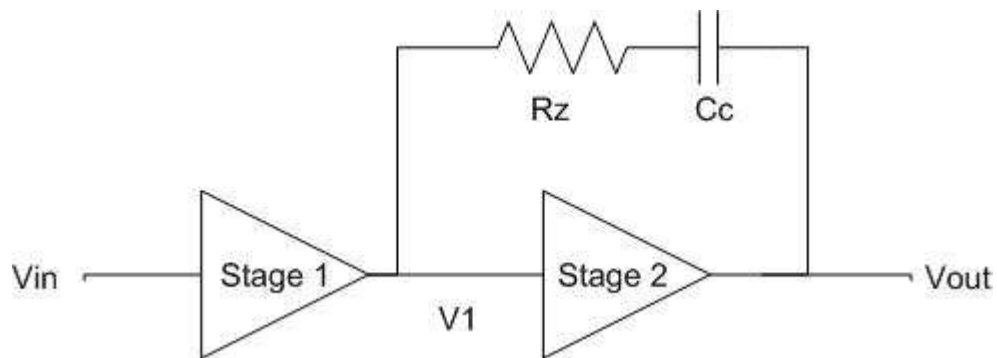
Fig. 3.3.3. Compensation circuit.

The Miller effect can be defined as the increase in the effective capacitance of the input of second stage because of the amplification through the feedback path created by the Miller capacitance. The associated pole due to Miller capacitor moves near the origin of the complex frequency plane and acts as a dominant pole. This reduces the bandwidth of the amplifier while improving the phase margin. Another advantage of the Miller effect is that the output pole of the system moves further away from the origin of the complex frequency plane due to the pole splitting technique. This reduces the output resistance of the circuit and improves the op amp stability.

The capacitance C_c in the feedback path produces a zero in the right-half portion of the complex frequency plane. This right-half plane (RHP) zero increases the magnitude and decreases the phase and behaves like a left-half plane (LHP) pole and a left-half plane zero. Thus, by selecting the value of the nulling resistor R_z the effect of the RHP zero has been minimized. This increases the gain bandwidth by moving all the poles and zeros except the dominant pole away from the unity-gain bandwidth frequency. The small-signal model of the system with the compensation circuit is shown in Fig. 3.3.4. Fig. 3.3.5 is the electrical equivalent circuit of Fig. 3.3.4.
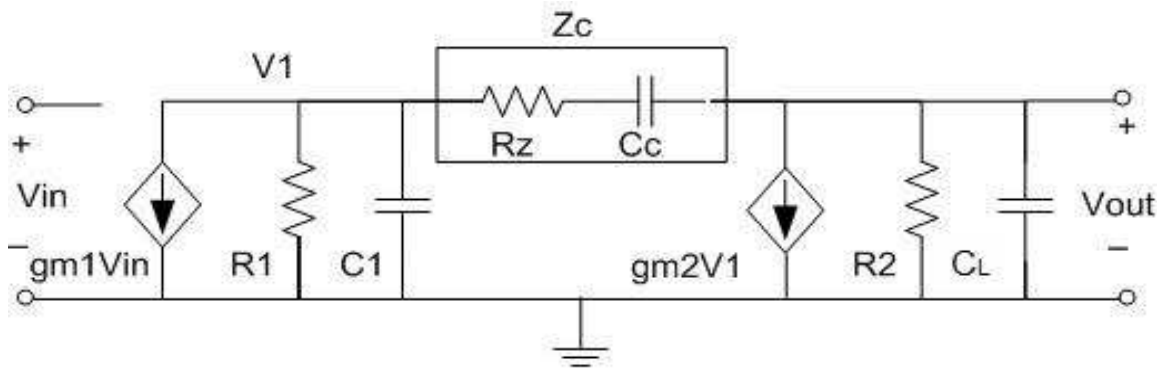
Fig. 3.3.4. Small-signal model of two-stage op amp with Miller compensation.
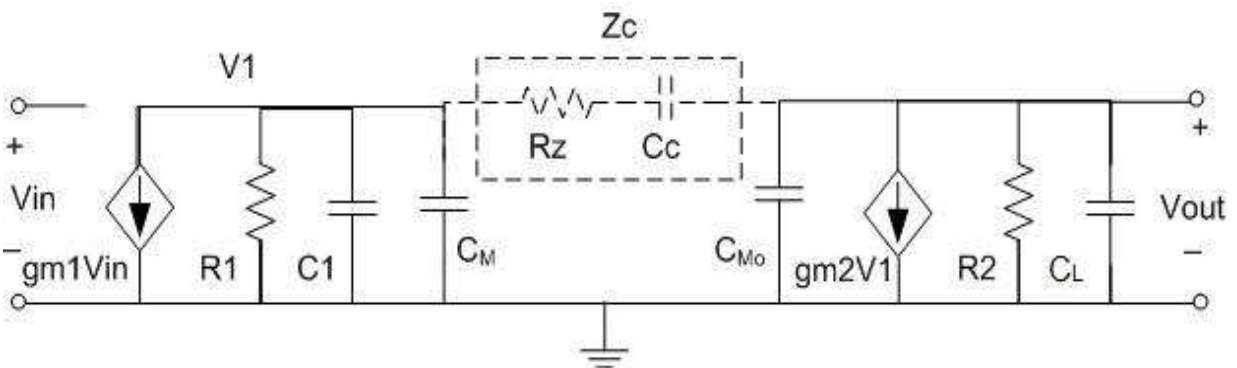
Fig. 3.3.5. Electrical equivalent model of two-stage op amp.

19

The additional input impedance due to Miller effect is Z_M and the additional output impedance is Z_{Mo}.

$$Z_M = {}^{Zc}/_{1 - A_o}$$ (3.1)

$$Z_{Mo} = {}^{Zc}/_{\left(1 - \frac{1}{A_o}\right)}$$ (3.2)

$$A_o = \frac{Vout}{V1}$$ (3.3)

$$C_M = s\,Cc\,\frac{1 - A_o}{1 + s\,Cc\,Rz}$$ (3.4)

$$C_{Mo} = s\,Cc\,\frac{1 - 1/A_o}{1 + s\,Cc\,Rz}$$ (3.5)

Now applying Kirchhoff's Current Law, following node voltages are obtained:

$$gm_1 Vin + \frac{V1}{R1} + s\,C1\,V1 + \left(\frac{s\,Cc}{1 + s\,Cc\,Rz}\right)(V1 - Vout) = 0$$ (3.6)

$$gm_2 V1 + \frac{Vout}{R2} + s\,C_L\,Vout + \left(\frac{s\,Cc}{1 + s\,Cc\,Rz}\right)(Vout - V1) = 0$$ (3.7)

The small-signal transfer function of the circuit has been given by using Cramer's rule,

$$\frac{Vout(s)}{Vin(s)} \approx \frac{g_{m1}g_{m2}R_1R_2\left\{1 - s\,Cc\left[\left(\frac{1}{gm2}\right) - Rz\right]\right\}}{1 + sg_{m2}R_1R_2C_c + s^2R_1R_2(C_1C_L + C_1C_c + C_cC_L) + s^3R_1R_2R_zC_1C_LC_c}$$ (3.8)

$$A_o = g_{m1}g_{m2}R_1R_2$$ (3.9)

The op amp's poles and zero can be found to be in (3.10) – (3.13). Here p_1 is the dominant pole frequency.

$$p_1 \cong -\frac{1}{g_{m2}R_2R_1C_c} \tag{3.10}$$

$$p_2 \cong -\frac{g_{m2}C_c}{C_1C_L + C_cC_1 + C_cC_L} \cong -g_{m2}/C_L \tag{3.11}$$

$$p_3 = -1/R_zC_1 \tag{3.12}$$

$$z_1 = \frac{1}{C_C\left(\dfrac{1}{g_{m2}} - R_z\right)} \tag{3.13}$$

The unity-gain bandwidth also known as gain bandwidth (GB) can be defined as,

$$GB = A_0 |p_1| = \frac{g_{m1}}{C_c} \tag{3.14}$$

For the required phase margin of 45°, the zero has been placed 10 times higher than GB. Thus, the relation between the highest non-dominant pole (p_2) and the GB can be represented as,

$$|p_2| \geq 2.2 \; GB \tag{3.15}$$

$$C_c > 2.2\frac{g_{m1}}{g_{m2}}C_L \tag{3.16}$$

The conditioning of the RHP has been done by making the RHP zero the same as the highest non-dominant pole. This way the zero cancels the pole and the circuit maintains good stability even with a large load capacitance.

$$z_1 = p_2 \tag{3.17}$$

$$R_z = \left(\frac{C_c + C_L}{C_c}\right)\left(\frac{1}{g_{m2}}\right) \tag{3.18}$$

3.3.2   Differential Input Stage

The differential input stage has N-channel MOSFETs (NMOS) (M1 & M2) as a differential input pair or a source coupled pair as shown in the Fig. 3.3.6. A P-channel MOSFET (PMOS)

current mirror load, consisting of M3 & M4, is placed at the top. The purpose of the current mirror is to create a current to voltage conversion stage. The biasing of the source coupled pair is done with a current sink (M5) placed at the bottom. The gate of the M5 transistor is connected with an external voltage source for fine tuning the biasing voltage.
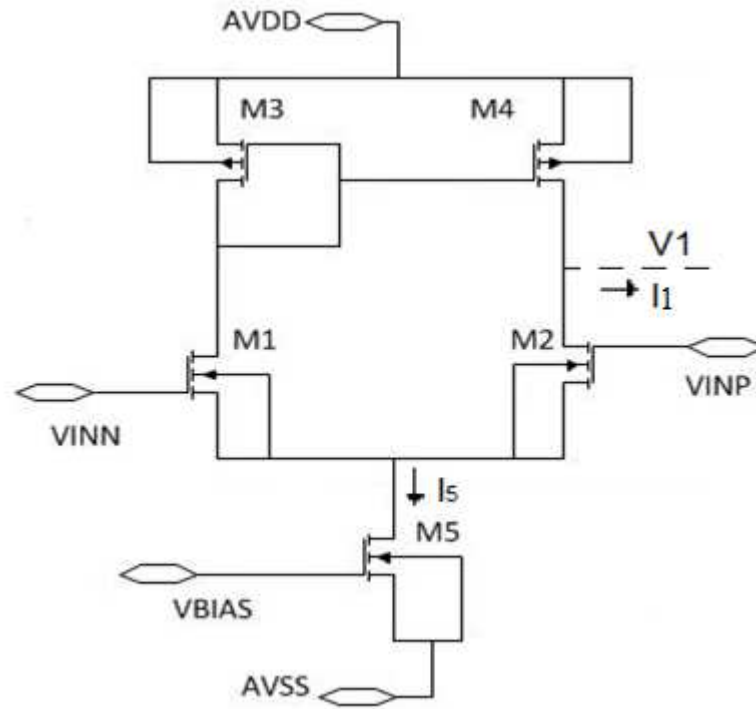
Fig. 3.3.6. Differential input stage.

When all the transistors are in saturation region and the differential input signal is zero the current at the output node, I_1, will be zero and the input device currents will be the same in both input branches and equal to $I_5/2$. This current along with the Miller capacitor C_c decides the internal slew rate (*SR*), which is given below,

$$SR = \frac{I_5}{C_c} \tag{3.19}$$

The process parameters are given in the table below.

22

TABLE 3.2 PROCESS PARAMETERS

Parameter	NMOS		PMOS	
	Channel Length L = 2 µm	Channel Length L = 5 µm	Channel Length L = 2 µm	Channel Length L = 5 µm
Threshold Voltage (V_T)	2.9 V	3 V	-3.45V	-3.65 V
Transconductance Parameter (K')	1 µA/V^2	0.8 µA/V^2	0.46 µA/V^2	0.3 µA/V^2
Channel Length Modulation (λ)	0.733 V^{-1}	0.733 V^{-1}	0.493 V^{-1}	0.493 V^{-1}

The W/L ratios of the transistors are calculated by implementing the drain current equations and the process parameters. The drain current equation of an n-channel MOSFET is given below,

$$I_d = \frac{1}{2} K_n' \frac{W}{L} (V_{GS} - V_{tn})^2 \tag{3.20}$$

The drain current equation of a p-channel MOSFET is given below,

$$I_d = \frac{1}{2} K_p' \frac{W}{L} (V_{Sg} - |V_{tp}|)^2 \tag{3.21}$$

The equations for the transconductance (g_m), transistor's drain to source resistance and transistor's saturation voltage between the drain-source are represented below,

$$g_m = \sqrt{2K' \left(\frac{W}{L}\right) I_d} = \frac{2I_d}{V_{DS(sat)}} \tag{3.22}$$

$$r_{ds} = \frac{1}{g_{ds}} = \frac{1}{I_d \lambda} \tag{3.23}$$

$$V_{DS(sat)} = V_{GS} - |V_t| = \sqrt{\frac{2I_d}{K'\left(\frac{W}{L}\right)}} \qquad (3.24)$$

The Input Common Mode Range (ICMR) of the circuit is determined by the NMOS input pair. The maximum limit of the ICMR, V_{IC} *(max)* is determined by the saturation voltage limit of the M3 & M4 transistors. The maximum common mode input voltage can be represented from [6] as

$$V_{IC}(max) = AVDD - V_{SD3} - |V_{tp3}| + V_{tn1} \qquad (3.25)$$

$$V_{IC}(\text{max}) = 15\,V - 0.55\,V - 3.45\,V + 2.9\,V = 13.9\,V \qquad (3.26)$$

The minimum ICMR is limited by the saturation voltages of the M1, M2 and the M5 transistors. The minimum common mode input voltage, V_{IC} (min), can be represent from [6] as,

$$V_{IC}(min) = AVSS + V_{DS5}(sat) + V_{DS1} + V_{tn1} \qquad (3.27)$$

$$V_{IC}(min) = 0\,V + 1.19\,V + 0.85\,V + 2.9\,V = 4.94\,V \qquad (3.28)$$

Thus, the total input common mode range can be expressed as $4.94\,V \leq V_{IC} \leq 13.9\,V$, which is very close to the specified ICMR.

The majority of the open loop voltage gain ($\approx$40 dB) has been achieved in the input stage. The small-signal analysis of the input stage differential amplifier has been performed to calculate the small-signal voltage gain and output resistance of the input stage. Fig. 3.3.7 shows the small-signal model of the input stage. Here the input branches have been assumed as perfectly matched on both sides.
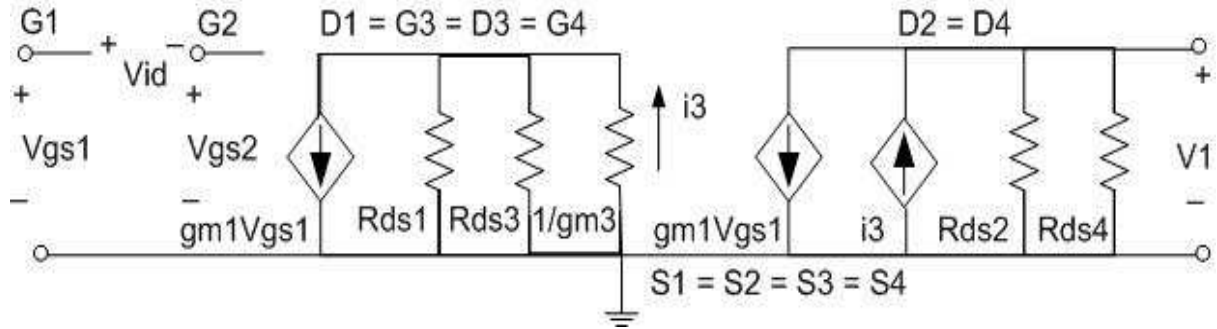
Fig. 3.3.7. Small-signal model of the input stage.

From the model the small-signal voltage gain can be calculated as shown in Eq. (3.29). The differential analysis has been done for the differential input signal V_{id}. Assuming ideal matching and symmetry, $g_{m1} = g_{m2}$, the output resistance is the sum of the parallel drain to source resistances of R_{ds2} and R_{ds4}. The relations between the voltage gain, output resistance and transconductance are shown below.

$$\frac{V_1}{V_{id}} = \frac{g_{m1}}{g_{ds2} + g_{ds4}} = g_{m1}(R_{ds2} \parallel R_{ds4}) \tag{3.29}$$

3.3.3   Common-Source Output Stage

The input stage is followed by an unbuffered, common source output stage. Most of the DC gain is achieved in the input differential stage. The purpose of the output stage is to further increase the dc gain and increase the output swing. In this stage the signal is driven into a capacitive output load. Fig. 3.3.8 shows the schematic of the unbuffered output stage. Here the input signal of this stage is the output of the first stage (V1).
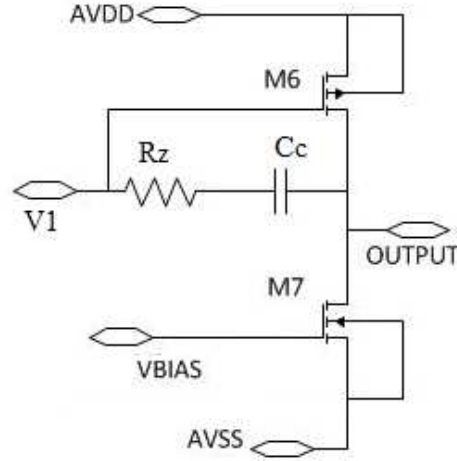
Fig. 3.3.8. Common-source output stage.

When the differential input equals to zero, the output should also be zero so that the op amp does not have any systematic input offset voltage. This means when $I_2 = I_4 = \frac{1}{2} I_5$, the output amplifier currents I_6 and I_7 should be equal.

For proper biasing, all of the transistors in Fig. 3.3.1 have to be in saturation. The pair M4, M6 and the pair M5, M7 create two mirroring currents. Now, to have proper mirroring between M4 and M6, $V_{SG4} = V_{SG6}$. And to have proper mirroring between M5 and M7, $V_{GS5} = V_{GS7}$.

$$If\ V_{SG4} = V_{SG6}, then\ I_6 = \frac{I_4}{\left(\frac{W}{L}\right)_4}\left(\frac{W}{L}\right)_6\ and\ \left(\frac{W}{L}\right)_6 = \left(\frac{W}{L}\right)_4\frac{g_{m6}}{g_{m4}} \tag{3.30}$$

$$If\ V_{GS5} = V_{GS7}, then\ I_7 = \frac{I_5}{\left(\frac{W}{L}\right)_5}\left(\frac{W}{L}\right)_7 \tag{3.31}$$

$$I_6 = I_7 \tag{3.32}$$

$$\frac{\left(\frac{W}{L}\right)_6}{\left(\frac{W}{L}\right)_4} = \frac{2\left(\frac{W}{L}\right)_7}{\left(\frac{W}{L}\right)_5} \tag{3.33}$$

26

The maximum and minimum output swing of the op amp are determined from the output stage. The maximum output swing is limited by the minimum saturation drain-to-source voltage of M6 before going to the active region. The minimum output swing is limited by the minimum saturation drain-to-source voltage of M7 before going to the active region.

$$V_{out(max)} = V_{DD} - V_{SD6(sat)} \tag{3.34}$$

$$V_{out(max)} = 15\,V - 0.7\,V = 14.3\,V \tag{3.35}$$

$$V_{out(min)} = V_{SS} + V_{DS7(sat)} \tag{3.36}$$

$$V_{out(min)} = 0\,V + 1.4\,V = 1.4\,V \tag{3.37}$$

Using the small-signal model, the small-signal output resistance and small-signal voltage gain of the output stage can be calculated. The small-signal model of the common source amplifier stage is presented in Fig. 3.3.9 below.
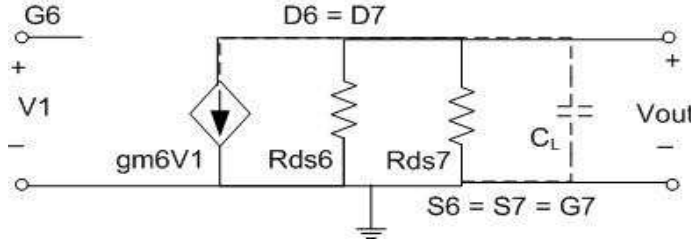
Fig. 3.3.9. Small-signal model of common source output stage.

Considering $g_{m6} = g_{m2}$ the small-signal voltage gain and resistance equation is shown below.

$$\frac{V_{out}}{V_1} = \frac{g_{m2}}{g_{ds6} + g_{ds7}} = g_{m2}(R_{ds6} \parallel R_{ds7}) \tag{3.38}$$

Thus the overall op amp gain can be represented as,

$$\frac{V_{out}}{V_1} * \frac{V_1}{V_{id}} = \frac{g_{m1}g_{m2}}{(g_{ds2} + g_{ds4})(g_{ds6} + g_{ds7})} = g_{m1}g_{m2}R_1R_2 \tag{3.39}$$

27

$$\frac{V_{out}}{V_1} * \frac{V_1}{V_{id}} = 80 \; dB \tag{3.40}$$

And the total power dissipation of the circuit can be represent as,

$$P = (I_5 + I_6)(V_{DD} + |V_{ss}|) \tag{3.41}$$

$$P = (50 + 260) \; \mu A * 15 \; V = 4.65 \; mW \tag{3.42}$$

The BSIM3 device model developed for the SiC process was used for simulation. The scalability of this model was limited such that the allowable width (W) of each of the transistors was set to a fixed value (20 µm) and the value of the length (L) was selected as either 2 µm or 5 µm depending on the transistor functions. For example, the L = 2 µm devices have higher transconductance (g_m) values, so they are good for devices which need high gain. The L = 5 µm devices have higher output resistance, which makes them better for matching circuits where the current stays constant with the changes in the drain voltage. For this the NMOS source coupled pair (M1 and M2) and the PMOS current mirror load (M3 and M4) of the 1st stage and the PMOS (M6) of the 2nd stage have device length L = 2 µm and the current sink of the 1st stage and the NMOS (M7) of the 2nd stage have device length L = 5 µm.

The value of the compensation capacitor was calculated as 3 pF. The calculated tail current of first stage was 50 µA and the calculated current in the second stage was 260 µA. The (W/L) ratios of the NMOS source coupled pair were calculated as 70 from *GB* specifications. And the (W/L) ratios of the PMOS current mirror and the NMOS current sink were calculated from the ICMR specifications as 360 and 88 respectively. For the required phase margin the non-dominant poles has been placed at least 10 times the *GB*. From this the (W/L) of the PMOS (M6) acquired as 3726. The (W/L) of the NMOS (M7) were calculated from the systematic offset requirement as 263. Lastly the value of the nulling resistor R_z has been calculated by using the

equation (3.18) as 4.6 kΩ. The frequency of the dominant pole along with other significant poles

and the zero of the system have been calculated as follows:

$$p_1 \cong -\frac{1}{g_{m2}R_2R_1C_c} = 14.62 \ kHz \tag{3.43}$$

$$p_2 \cong -\frac{g_{m2}C_c}{C_1C_L + C_cC_1 + C_cC_L} \cong -\frac{g_{m2}}{C_L} = 94.28 \ MHz \tag{3.44}$$

$$p_3 = -\frac{1}{R_zC_1} = 141.31 \ MHz \tag{3.45}$$

$$z_1 = \frac{1}{C_C\left(\dfrac{1}{g_{m2}} - R_z\right)} = 102.81 \ MHz \tag{3.46}$$

The calculated values of the transistors and the values of the compensation capacitor and

nulling resistor are then optimized using simulation. The calculated values and the actual values

of the size of the transistors and passive elements are given in TABLE 3.3 below.

TABLE 3.3 DEVICE SIZES

	Calculated Value	Actual Value	CDF Parameter	
			(W/L)	Fingers
(W/L)$_1$ and (W/L)$_2$	177.80	70	20/2	7
(W/L)$_3$ and (W/L)$_4$	359.32	360	20/2	36
(W/L)$_5$	50.73	88	20/5	22
(W/L)$_6$	3726.71	2240	20/2	224
(W/L)$_7$	263.08	264	20/5	66
C$_c$	3 pF	2.196 pF	---	---
R$_z$	4595.96 Ω	7666.67 Ω	---	---

CHAPTER 4

SIMULATION OF THE OPERATIONAL AMPLIFIER

The performance of the designed op amp was evaluated and optimized by simulation. Test benches were developed to verify different circuit characteristics performance over different process corners (Typical, Fast-Fast, Slow-Slow) and over temperature (25 °C to 275°C). These variations in the process corners imply different drive strengths of the NMOS and PMOS transistors. For example a fast-fast corner means both the NMOS and PMOS transistors have low threshold voltages. The simulations were run using the Synopsys HSPICE simulator. The utilized models were developed based on BSIM3 device models and the high fidelity process design kit was created as part of NSF-BIC project. The simulation setup, design tool chain and the AC, DC and transient performance analysis will be presented in this chapter.

4.1   Simulation Setup

The simulation setup was created to measure and verify every performance characteristics (DC, AC and transient responses) of op amp in a close approximation of real world environments. Every test bench was designed to calculate some specific performance of the op amp and for this, additional passive elements such as resistors and capacitors were included to recreate a real life test setup. The schematics of the test setups include the input signals, power supply, the input bias voltage and the output load capacitance for each test circuit. Due to the high threshold voltages of the transistors in SiC, the power supply is 15 V, the bias voltage for

every simulation was calculated as 4.45 V and the common mode voltage V_{ICM} was taken as 7 V or around mid-rail.

4.2 DC Simulation

DC simulation was used to characterize the following specifications: input offset voltage, the DC power dissipation, the input common mode range and the output voltage range (OVR). The test bench configuration for input offset measurement is shown in Fig. 4.2.1. The load capacitance was set to 10 pF since the input capacitance of the probes of the Tektronix TDS 744A oscilloscope used for post-fabrication testing are in that range.
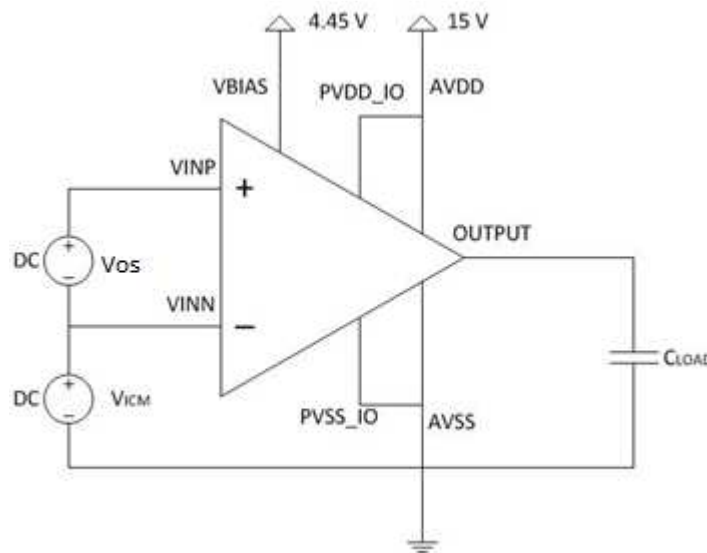
Fig. 4.2.1. Input offset voltage measurement.

For the offset measurement, the DC power supply V_{ICM} was set at 7.5V and the DC power supply V_{OS} was swept from –0.1 V to 0.1 V. The simulation results for different temperatures are shown in Fig. 4.2.2. When the output voltage was 7.5 V the voltage V_{OS} at the input is the offset value. But the input V_{OS} at that time is very close to 0 V, as expected. This is because the simulations do not account for transistor mismatch that exists in the actual circuit. So, even

31

though there seems no significant offset voltage present in the simulation, in real life testing some offset will be present.
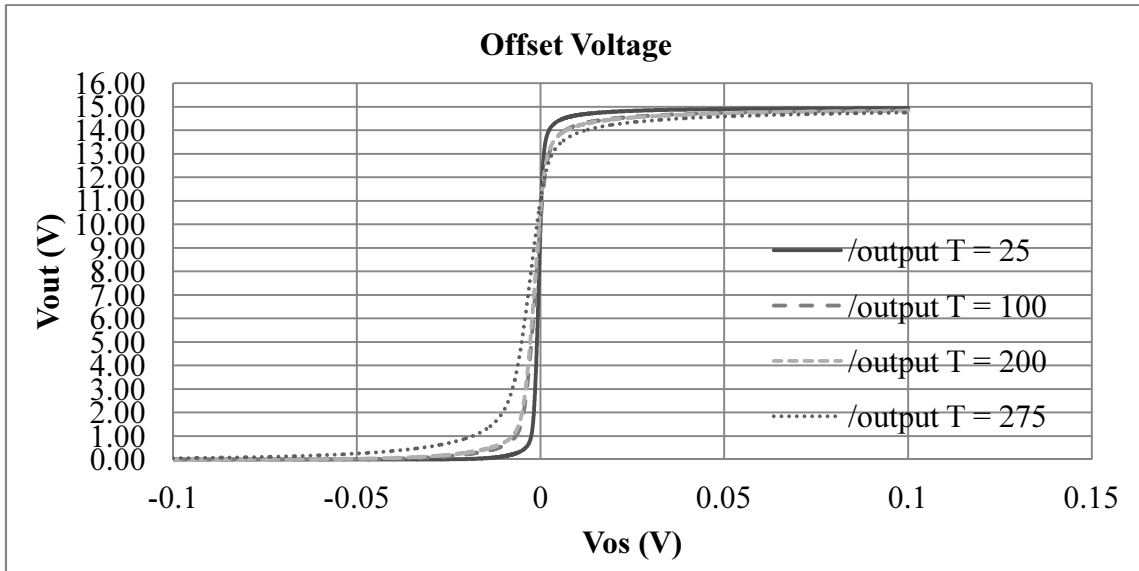
Offset Voltage

Fig. 4.2.2. Simulation results of input offset voltage and output voltage swing.

The next DC characteristics that were simulated were the ICMR and OVR. Fig. 4.2.4 shows the test setup configuration. Here the op amp is placed in a voltage-follower configuration.
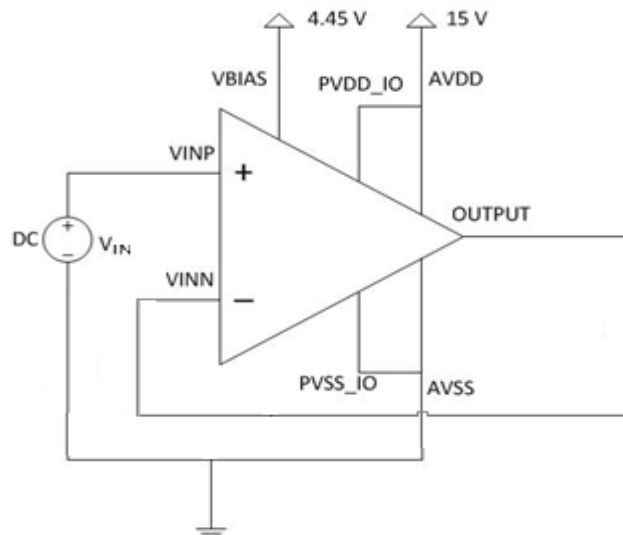
Fig. 4.2.3. Op amp in voltage-follower configuration.

In the voltage follower configuration (as a unity-gain buffer), the output of the amplifier is connected with its negative input. This forces the output to be equal to the input voltage when the op-amp functions. The simulation results of the voltage follower at 25 °C and at 275 °C are shown in Fig. 4.2.4 and Fig. 4.2.5 respectively.
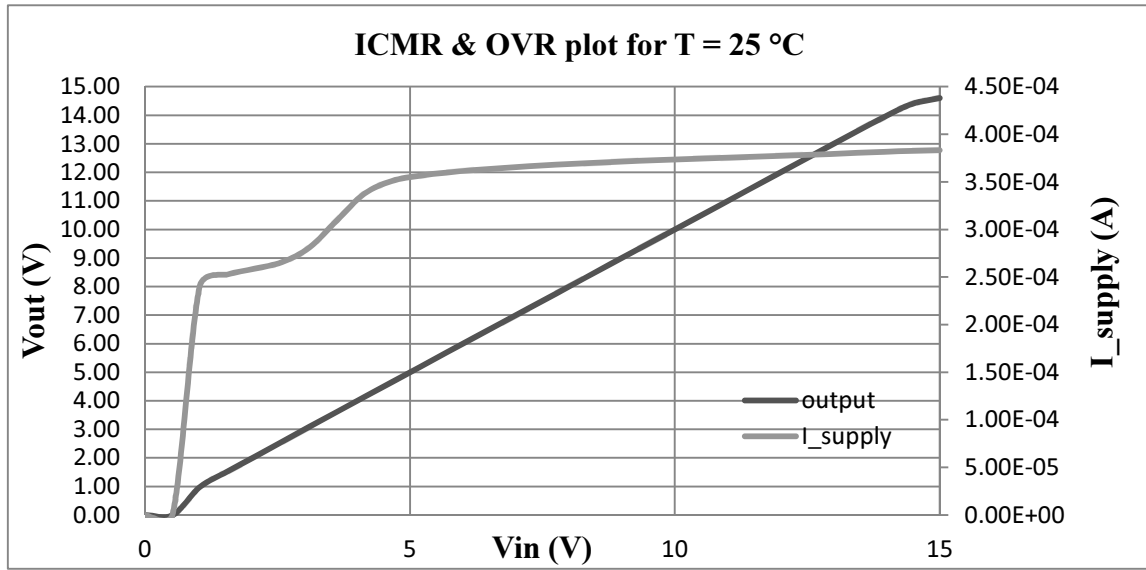
Fig. 4.2.4. Simulation results of voltage follower at T = 25 °C.
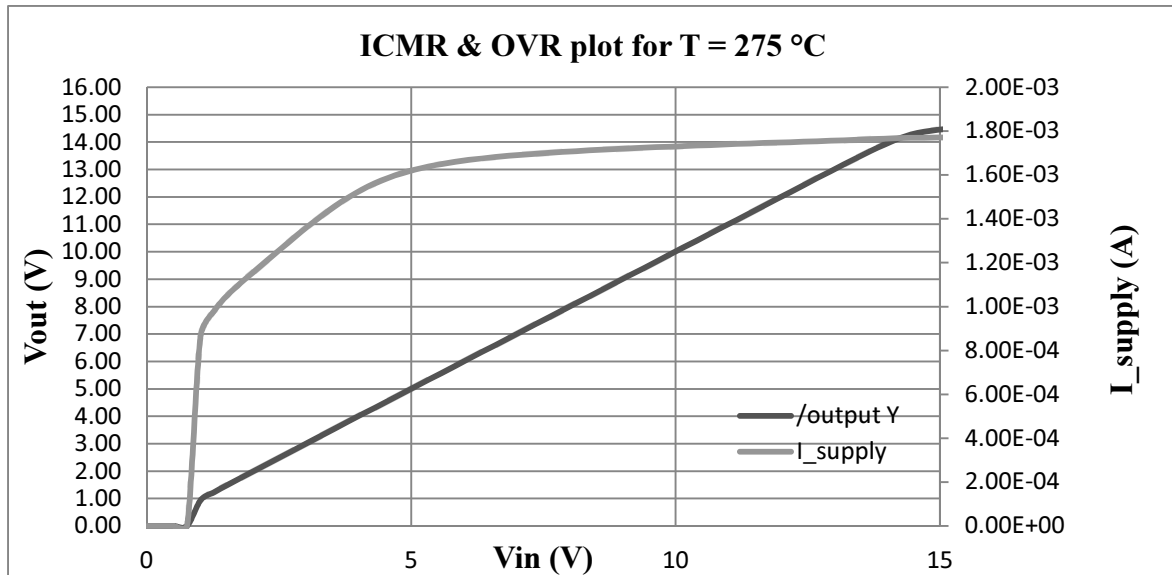
Fig. 4.2.5. Simulation results of voltage follower at T = 275 °C.

From the simulation data the ICMR of the op amp was found to be 4.7 V to 14.58 V at 25 °C and 4.87 V to 14.22 V at 275 °C. The OVR at 25 °C is 690 mV to 14.45 V and at 275 °C is 980 mV to 14.12 V. But in the open loop configuration, the maximum allowable input common mode voltage (14.58 V at 25 °C and 14.22 V at 275 °C) does not provide acceptable gain (gain is less than 55dB). So for the open loop mode, the maximum input common mode voltage is 13.7 V at 25 °C and 10.34 V at 275 °C (allowing at least 55dB gain). At room temperature the ICMR is within the specification but at the high temperatures the threshold voltages of the transistors shifts and the maximum input common mode voltages is less than the specifications.

The total DC power consumption was measured by measuring the dc current supply (I_supply) of the op amp at different temperatures. From the data the value of I_supply at 25 °C is found to be 365.52 µA and at 275 °C is found to be 1.69 mA. Thus, the power dissipation at 25 °C is 5.483 mW and at 275 °C is 25.35 mW, respectively. Fig. 4.6 represents the current sweep across temperature and Table 4.1 summarizes the overall DC simulation characteristics.
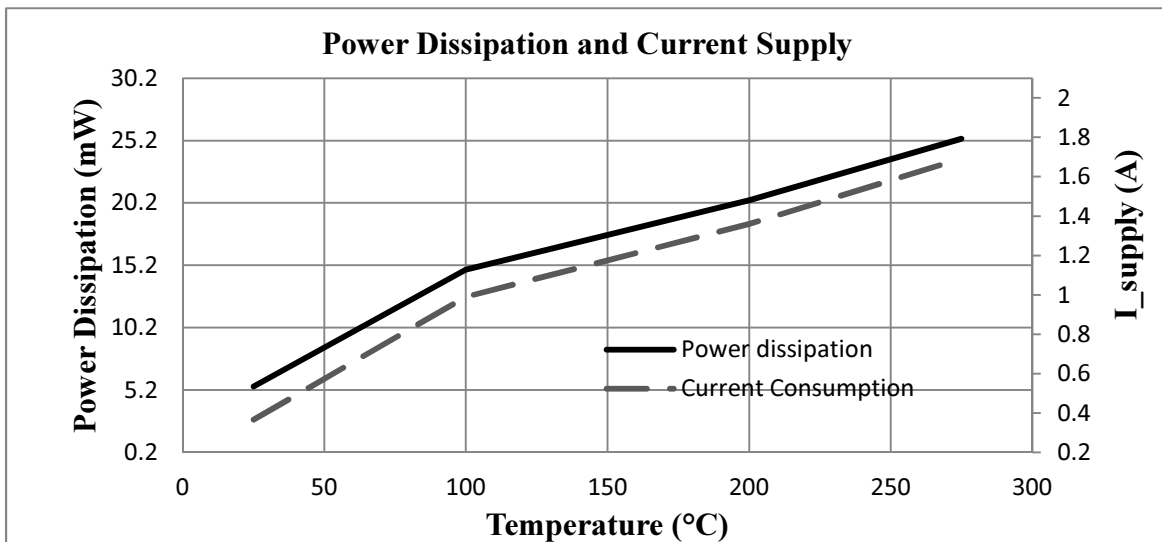
Fig. 4.2.6 The supply current sweet over temperature.

TABLE 4.1 DC SIMULATION CHARACTERISTICS

Parameter	Temperature	Simulated Value	Unit
Unity-gain mode ICMR	25	4.7 – 14.58	V
	100	4.62 – 14.12	
	200	4.45 – 14.34	
	275	4.87 – 14.22	
Open-loop mode ICMR	25	4.7 – 13.7	V
	100	4.62 – 12.178	
	200	4.45 – 12.1	
	275	4.7 – 10.34	
Output voltage swing range	25	0.69 – 14.45	V
	100	0.68 – 14.4	
	200	0.674 – 14.15	
	275	0.98 – 14.12	
Total current demand	25	0.366	mA
	100	0.99	
	200	1.361	
	275	1.691	
Power dissipation	25	5.49	mW
	100	14.85	
	200	20.42	
	275	25.35	

4.3   AC Simulation

AC simulation was used to characterize the following specifications: the open-loop gain, unity-gain bandwidth (GB) and phase margin. All of these characteristics were measured using a single test bench. The Fig. 4.3.1 shows the test bench setup for AC performance analysis. The unity-gain bandwidth is furthermore verified in transient simulations.
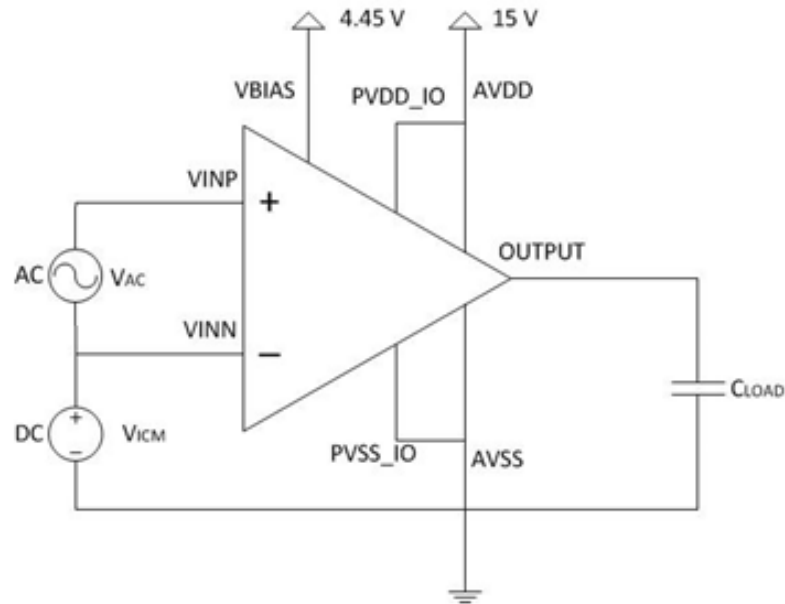
Fig. 4.3.1. Test bench setup for AC analysis.

The open-loop gain of the op amp is limited by the bandwidth of the amplifier. There is a tradeoff between the phase margin and the GB. To increase the phase margin, the GB and AC gain will decrease and if we increase the GB and AC gain, the system will become less stable.

In the TABLE 4.2 the AC simulated parameters for 25 °C, 100 °C, 200 °C and 275 °C has been presented. The simulations were executed using BSIM3 models. The simulations were run again using an updated BSIM4 model that was developed after the fabrication.

TABLE 4.2 AC SIMULATION CHARACTERISTICS

Parameter	Temperature (°C)	Simulated Value			Unit
		Typical	Fast-Fast	Slow-Slow	
Open loop gain	25	74.29	59.6	73.03	dB
	100	66.32	52.5	63.67	
	200	65.81	36.11	57.23	
	275	60.84	42.51	57.18	
Unity-gain Bandwidth	25	2.953	7.03	2.164	MHz
	100	5.895	9.487	4.216	
	200	5.985	9.221	5.747	
	275	6.224	9.954	6.556	
Phase Margin	25	40.65	36.4	38.4	(degree)
	100	42.93	36.1	40.6	
	200	45.11	50.8	41.5	
	275	42.1	50.1	41	

Fig. 4.3.2 and Fig. 4.3.3 represent the magnitude and phase plots for different temperatures using the BSIM3 model. But in the updated BSIM4 device model, some of the circuit performance declined: by 9% to 19% for open loop gain and 36% to 38% for phase margin; while some performances improved: by 40% to 55% for unity-gain bandwidth.
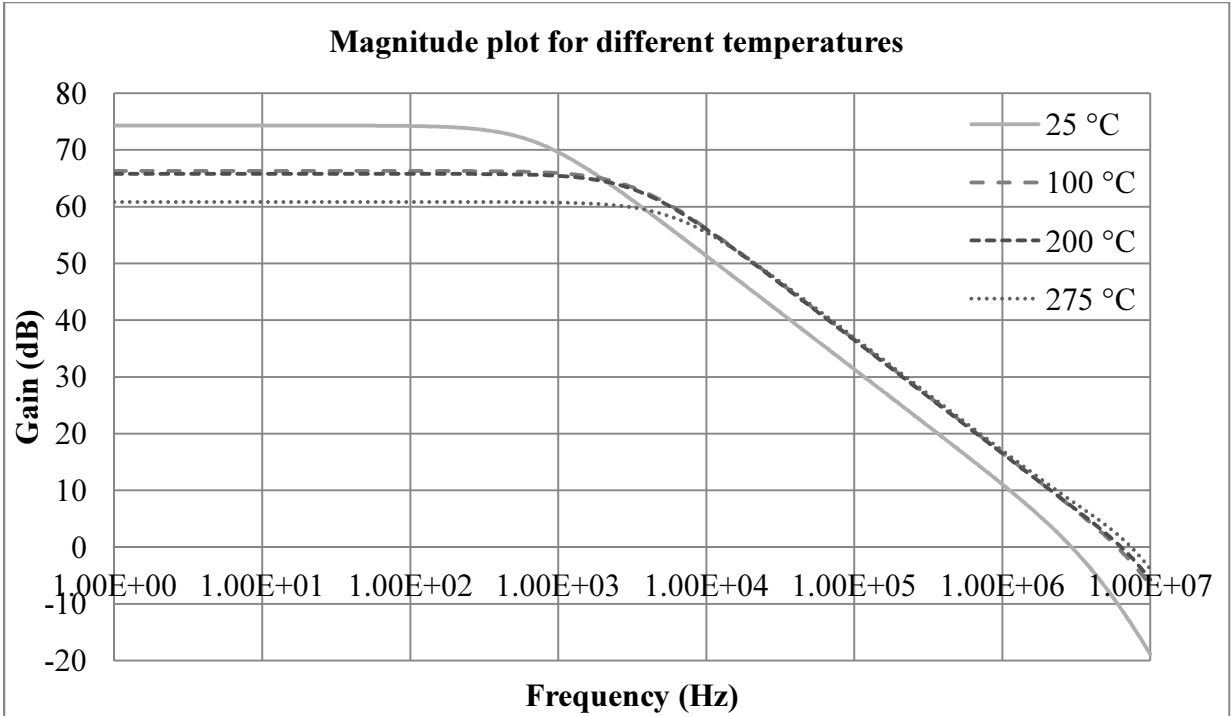
Fig. 4.3.2 Magnitude plot for different temperatures.
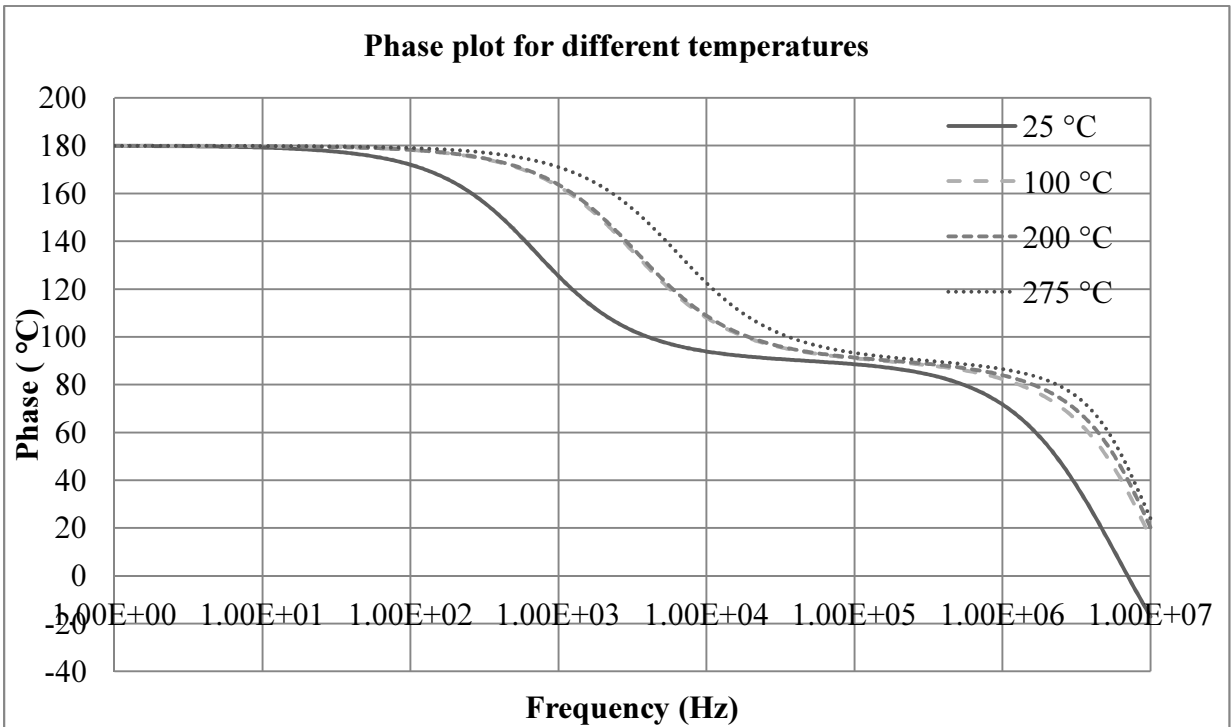
Fig. 4.3.3 Phase plot for different temperatures.

38

4.4   Transient Simulation

Transient simulation was used to characterize the following specifications: the closed-loop unity-gain bandwidth and the slew rate. The test bench setup for the transient analysis is shown in Fig. 4.4.1.
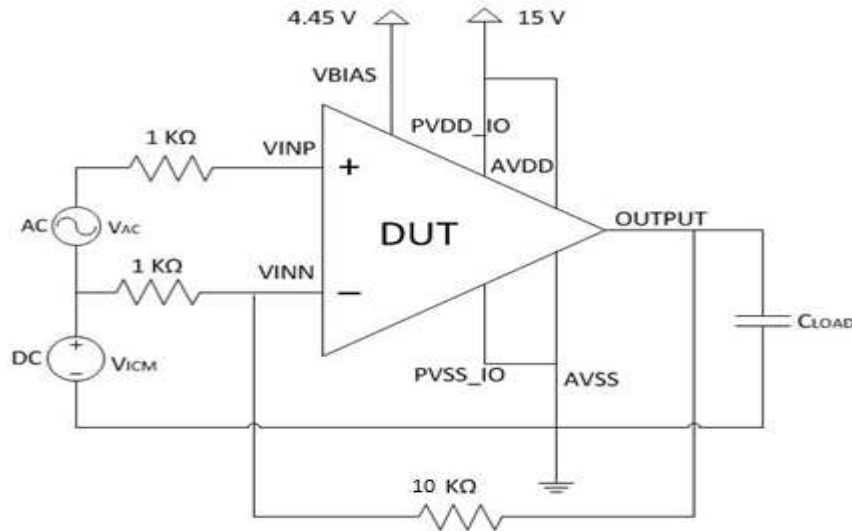
Fig. 4.4.1 Test bench for transient analysis.

To determine the closed-loop unity-gain bandwidth, the circuit was simulated with an external feedback path. The amplitude of the ac signal was 10 mVp-p and the initial frequency was 10 kHz. After this the frequency has been sweep until the output signal equals to input signal. This frequency is the unity-gain bandwidth. The closed-loop unity-gain bandwidth for 25 °C is 2.6 MHz and the closed-loop unity-gain bandwidth for 275 °C is 7.2 MHz.

For the slew rate measurement the sinusoidal source is replaced by a pulse generator and the feedback resistor replaced with a short. The frequency of the pulse signal was 10 kHz, the rise and fall time are 5 ns each and the pulse width is 50 µs. The modified test bench for slew rate is shown below in Fig. 4.4.2.
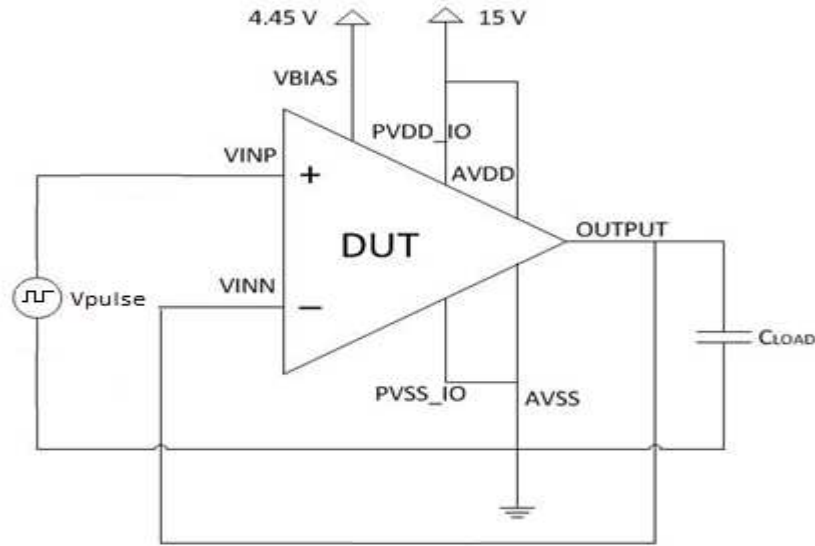
Fig. 4.4.2. Test bench for analysis of slew rate.

The slew rate is the fastest rate of change of the output voltage in response to a change of the input voltage. It is expressed as volts per microsecond. Table 4.3 shows the simulated results of the slew rate characteristics. For a fixed load capacitance of 10 pF, the supply current rises with temperature due to the shift in threshold voltages. For this the slew rate also increases with temperature. At all temperatures the simulated slew rate is higher than the *SR* specification of 10 V/µs.

TABLE 4.3 AC SLEW RATE VALUE FOR DIFFERENT TEMPERATURES

Temperature (°C)	Vmax (V)	Vmin (V)	Slew rate (V/µs)
25	14.6	0.066	26.41
100	14.27	0.056	71.35
200	14.33	0.27	76.6
275	14.45	0.35	95.88

CHAPTER 5

PHYSICAL DESIGN

The last step in the design process is the physical design or the layout. The toolchain for the layout is the Virtuoso Layout Editor in the Cadence design kit. The complete layout process includes the layout of the transistors with proper connections, the pin specification, the design rule check verifications and layout vs schematic check. After the layout, the op amp is placed inside the padframe and parametric extraction performed. Finally, the circuit is resimulated with the padframe to confirm the performance characteristics.

5.1   Chip Layout

The chip layout is divided into two stages: the differential input stage and the common source amplifier output stage. There are a total of eight pins associated with the layout: AVDD and AVSS for power supplies, VINP and VINN for positive and negative inputs, respectively, VBIAS for voltage biasing, PVDD_IO and PVSS_IO for power supplies to padframe and OUTPUT for the output. The Fig. 5.1.1 represents the layout of the op amp and the Table 5.1 represents the input and output pins of op amp and their description.
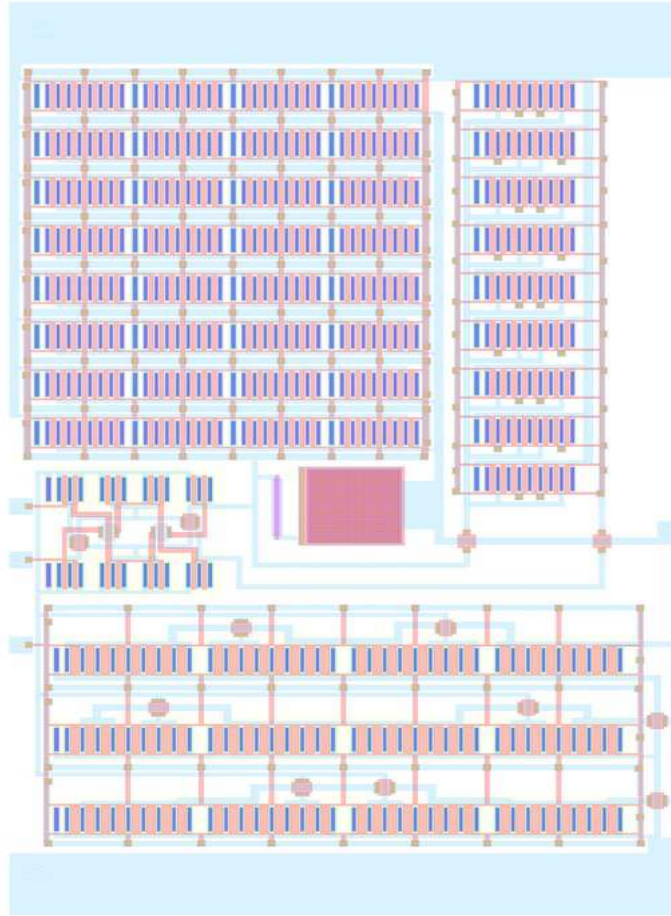
Fig. 5.1.1. The layout of the op amp (Length = 431.6 μm; Width = 738 μm).

TABLE 5.1 THE INPUT AND OUTPUT PINS OF OP AMP WITH DESCRIPTION

Pin Name	Pad Frame Name	Location	Connection Description
VINP	POTA2STG_VINP	Upper-left	Positive Input: 7.5 V DC + 1 V AC
VINN	POTA2STG_VINN	left	Negative Input: 7.5 V DC voltage
VBIAS	POTA2STG_VBIAS	Lower-Left	Desired Biasing Voltage: 4.45 V DC
OUTPUT	POTA2STG_OUTPUT	Right	Output

42

AVDD	PAVDD	Top	Power supply: 15.0 VDC
AVSS	PAVSS	Bottom	Circuit ground: 0 VDC
PVDD_IO	PVDD_IO	4 pads: each in one corner	Power supply to padframe: 15.0 VDC
PVSS_IO	PVSS_IO	4 pads: each in one corner	Ground to padframe: 0 VDC

The physical design is one of the important steps in the design. A circuit with good simulation performance can have unsatisfactory characteristics with substandard layout. One of the main key points with circuit layout is the need to have good matching between similar items [6]. One way to get this is to create a unit value of a paired device and repeat it multiple times as needed. This is called the "unit matching" principle. Another important principle to be considered is the "common-centroid" principle. In the common centroid principle two or higher matched devices are arranged in such a form that both of their axis of symmetry will overlap [15]. This type of layout is seen in the Fig. 5.1.2 with NMOS input pair transistor matching.
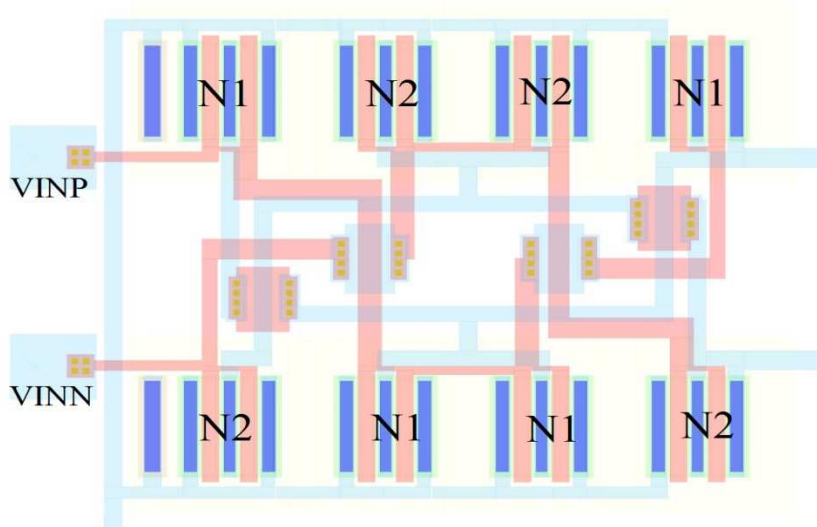
Fig. 5.1.2. NMOS input pair transistor matching.

The layout structure implements "inter-digitated arrays" or in other words, uses a single multi-fingered transistor to represent two or more transistors. The current mirror load of the differential input with M3 and M4 transistors (Ch. 3, Sec 3, Fig. 3.3.1) and the current mirror circuit with M5 and M7 transistors (Ch. 3, Sec 3, Fig. 3.3.1) are matched in the same way as shown in Fig. 5.1.3 and Fig. 5.1.4, respectively.
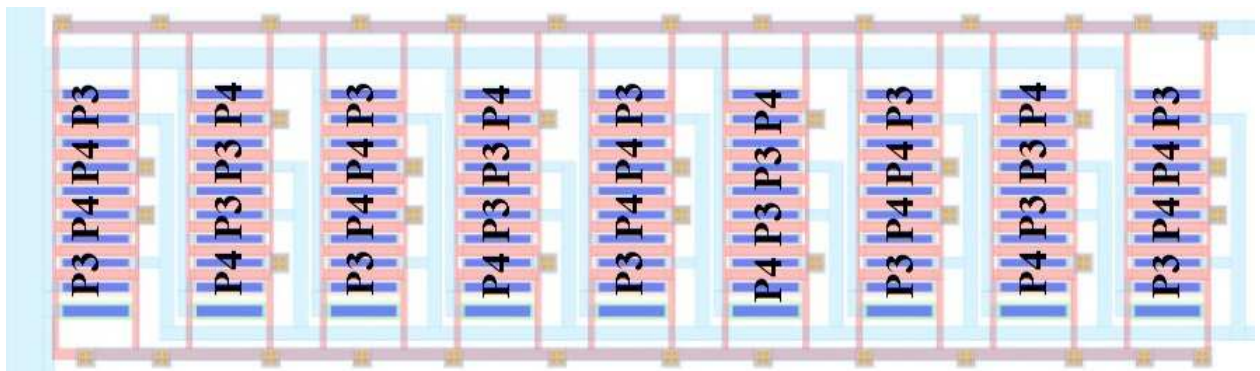
Fig. 5.1.3. Current mirror (M3 & M4) layout.
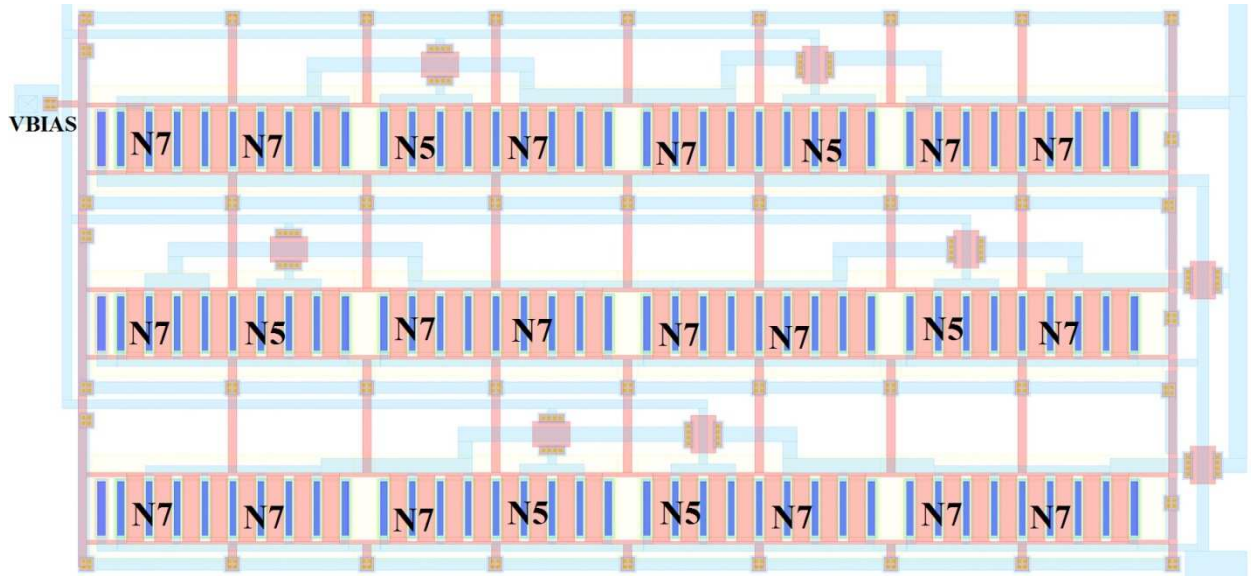
Fig. 5.1.4. Current mirror (M5 & M7) layout.

The transistor-matching layout of the op amp follows the layout rules for common-centroid layout design according to [15]. The rules are given below:

1. Coincidence: The placement of the matching transistors maintains the coincidence of their centroids.

2. Symmetry: The device array is symmetric in both X- and Y-axes.

3. Dispersion: The device segments are uniformly distributed

4. Compactness: The device is compacted as much as possible following the device rules.

A number of contacts are placed and large paths of the poly layer have been superimposed with metal layer to provide minimum resistance path. A large number of contacts have been placed in these paths as well.

The design rules check was performed throughout the layout process and layout versus schematic was used to confirm the proper connections in the device. Next, parasitic extraction of the op amp was performed and the actual parasitic capacitance and resistance values from the layout extracted. The op amp was resimulated with these extracted values to confirm its performance.

The final layout includes the padframe with eight analog pads for proper bond wiring, packaging and testing. The final layout with padframe and inputs & output bondpads is shown in Fig. 5.1.5 below.
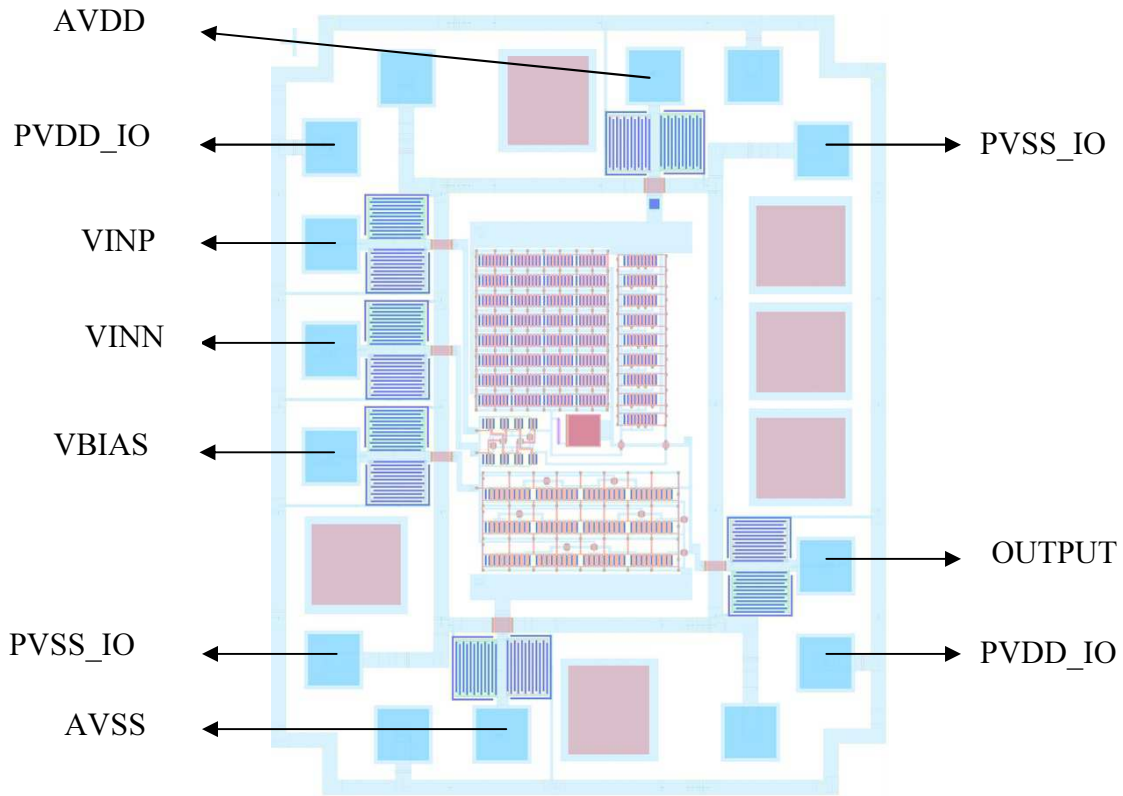
Fig. 5.1.5. Final chip layout with padframe and pin connections.

The full chip included over 40 analog, mixed-signal and digital building block circuits. The final chip size was 21 x 12.5 mm^2 and the chip was sent to fabrication on August 2013. The final area of the op amp including the padframe is 1200 μm X 1520 μm and the final circuit includes a total of seven transistors and one capacitor and one resistor. The die micrograph of the fabricated op amp is shown in Fig. 5.1.6.
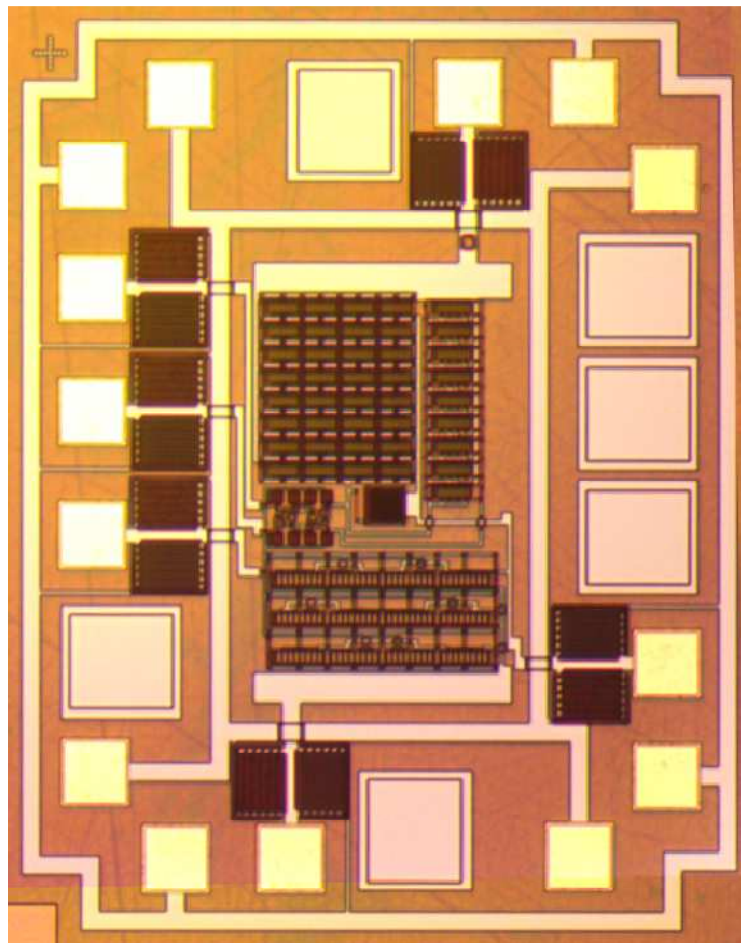
Fig. 5.1.6. Die micrograph of the fabricated op amp.

CHAPTER 6

TESTING AND CHARACTERIZATION

After the tapeout the die was sent for fabrication. Testing preparations such as test planning and packaging options were evaluated during this time. Since the main application of the circuit is in high temperature different bonding and packaging options that were compatible with the temperature range were considered. A detailed test plan was developed and printed circuit board created to reproduce the test benches used at the design and verification steps.

6.1   Bond Wire and Packaging

Due to the low pin count of the circuit, testing using a Semiprobe probe station was the primary choice. Exhaustive DC testing was performed using the probe station and Keithley 4200 Semiconductor Characterization System. But to measure the op amp transient performance in feedback circuitry packaging of the circuit was required.

The packaging and wire bonding was accomplished at the High Density Electronics Center (HiDEC) at the University of Arkansas. The first step was dicing of the op amp reticle from the fabricated 4" wafers. After this step, the die was attached into the cavity of a 64-pin ceramic quadpack package using high-temperature epoxy and the package was kept inside a vacuum oven for about 4 hours at 150 °C to cure the epoxy. The next step was wire bonding. The pads of the circuit were bonded to the package by using a 1 mil gold wire with a small gold ball formed by the bonder at the ends. The bonding plan for the op amp is shown in the Fig. 6.1.1 below.

Three op amps (along with one other circuit, a Schmitt trigger designed by a fellow student) were bonded in a single package. The pin out information is detailed in TABLE 6.1.
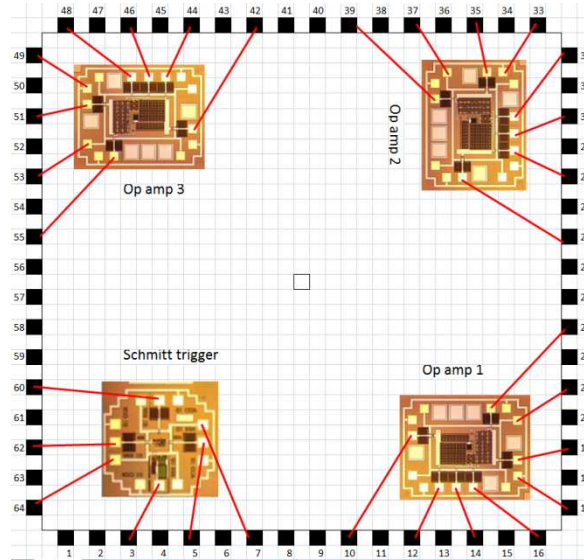
Fig. 6.1.1. Bonding plan.

TABLE 6.1 THE BONDING DIAGRAM PIN CONFIGURATIONS

Pin No.	Corresponding Signal	Pin No.	Corresponding Signal	Pin No.	Corresponding Signal
10	PAVDD	26	PAVDD	42	PAVDD
12	VINP	28	VINP	44	VINP
14	VINN	30	VINN	46	VINN
16	VBIAS	32	VBIAS	48	VBIAS
17	PVDD_IO	33	PVDD_IO	49	PVDD_IO
19	PAVSS	35	PAVSS	51	PAVSS
21	PVSS_IO	37	PVSS_IO	53	PVSS_IO
23	Output	39	Output	55	Output

The last step in the packaging process is the soldering of the package with the printed circuit board (PCB) as shown in Fig. 6.1.2. The PCB is made out of a high temperature Rogers material that is capable of high temperature testing (300 ^{o}C) using a hot plate as a heat source. Finally, all the solders and wire bonds were checked for shorts and the circuit readied for testing.
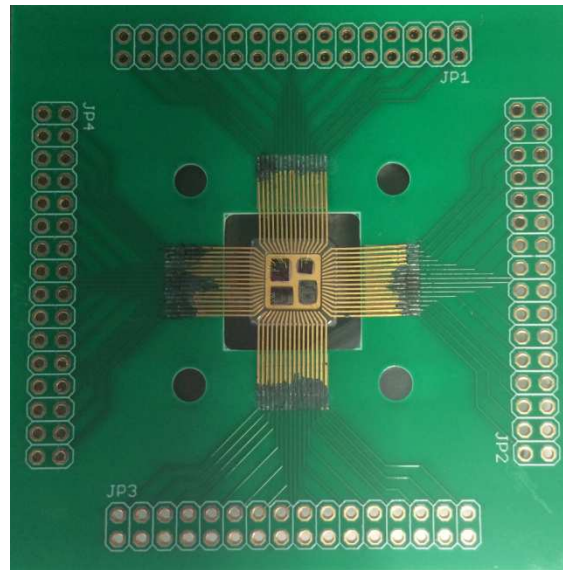
Fig. 6.1.2 Final packaged chip.

6.2   Test Setup

The testing of the op amp was done using both the probe station and PCB board setup. There are a total of eight input/output pins of the op amp including the power supply to the padframe. In the probe station eight probe tips were used to probe the eight pads as shown in the Fig. 6.2.1, using a combination of active and passive probes. The output of the probe tips were then connected with the appropriate equipment. This setup was used to measure the primary heartbeat tests: offset voltage, ICMR, OVR, gain and slew rate.
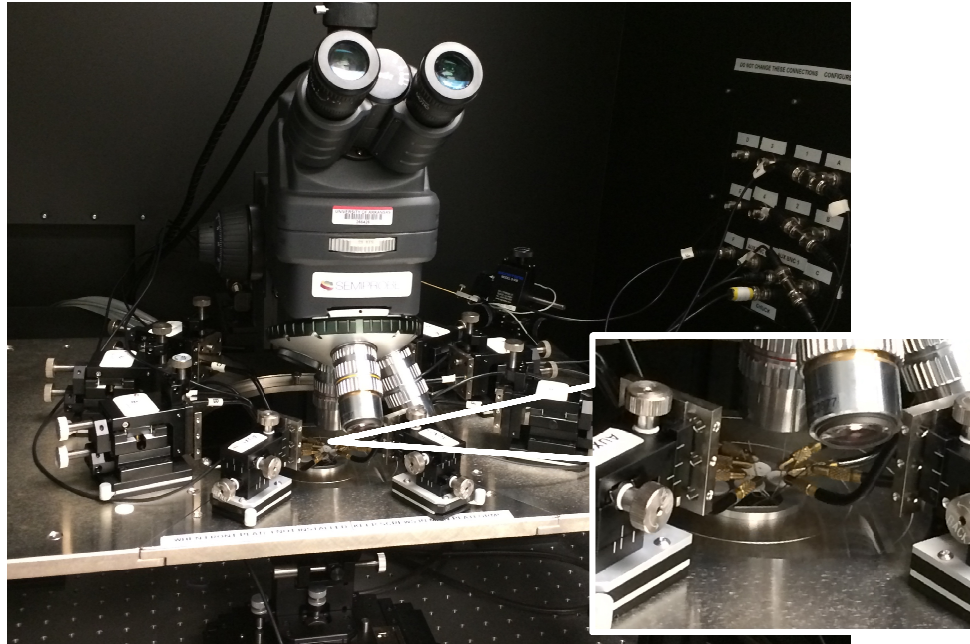
Fig. 6.2.1 Probe station test setup.

During the testing of the op amp using the PCB board setup, the packaged chip and the test setup were kept in two different PCB using a mother-daughter board setup and external connections were made between them. This was been done to facilitate high temperature testing where the packaged chip Rogers board placed in the hot plate is capable to withstand high temperature but not vice versa. Two test boards, one 1.5 inch x 2.5 inch and another 1.45 inch x 1.55 inch were developed using Eaglesoft PCB software as shown in Fig. 6.2.2.

The list of equipment used for testing is represented in TABLE 6.2. The test plan developed for each characteristic measurement along with the diagrams and connections are included in Appendix A.

TABLE 6.2 LIST OF TEST EQUIPMENT

Tektronix TDS 744A Oscilloscope
Tektronix AFG3022B Dual Channel Arbitrary/ Function Generator 25MHz
Agilent E3631A Triple Output DC Power Supply
Keithley Semiconductor Characterization System
Hewlett Packard 3458A Multimeter
Cole Parmer Stable Temp hotplate
Marconi Instrument 10KHz, 2.7GHz signal Generator 2031
Printed Circuit Board

(a)   (b)
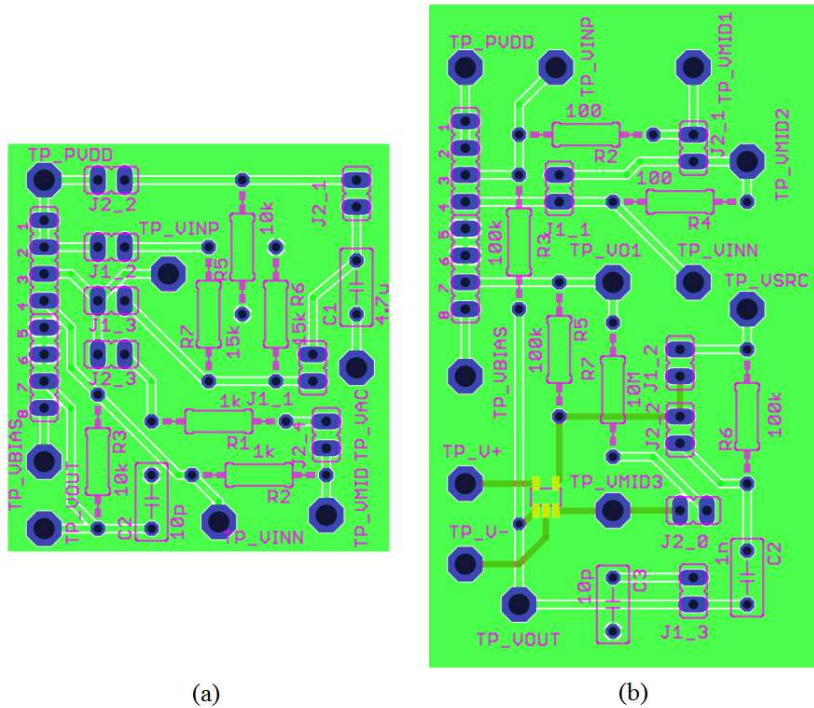
Fig. 6.2.2. PCB layout (a) 1.45" x 1.55" (b) 1.5" x 2.5".

6.3 Test Results

This section describes the actual performance of the designed circuit at different temperature ranges. The first test performed was a "heartbeat" test at the probe station. The purpose of this test was to observe that the circuit was functional. Die from different location of the wafer has been tested sporadically to check for functionality and the device yield was 100% although the dies in the edge of the wafer showed better transient performance than dies in the center due to their stronger PMOS and weaker NMOS properties. The Fig. 6.3.1 shows the wafer diagram where the shaded dies represent the tested circuits.
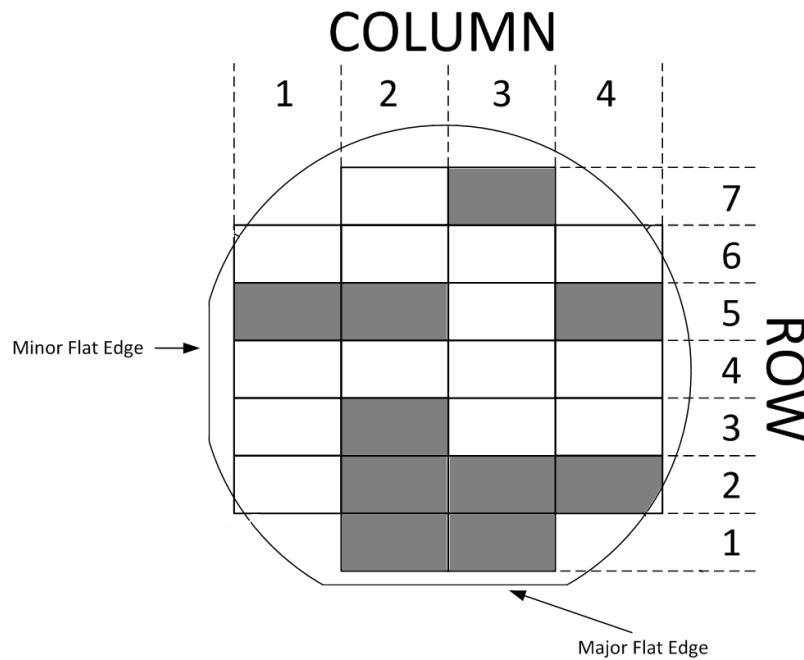
Fig. 6.3.1 Wafer diagram

Once functional circuits were identified, the next test performed was a bias sweep to measure the optimum bias voltage (the same range as the simulation Fig. 6.3.2). The input was provided

by a triangular wave from the function generator AFG 3022B and the plots were captured by Tecktronix TDS 744A oscilloscope.
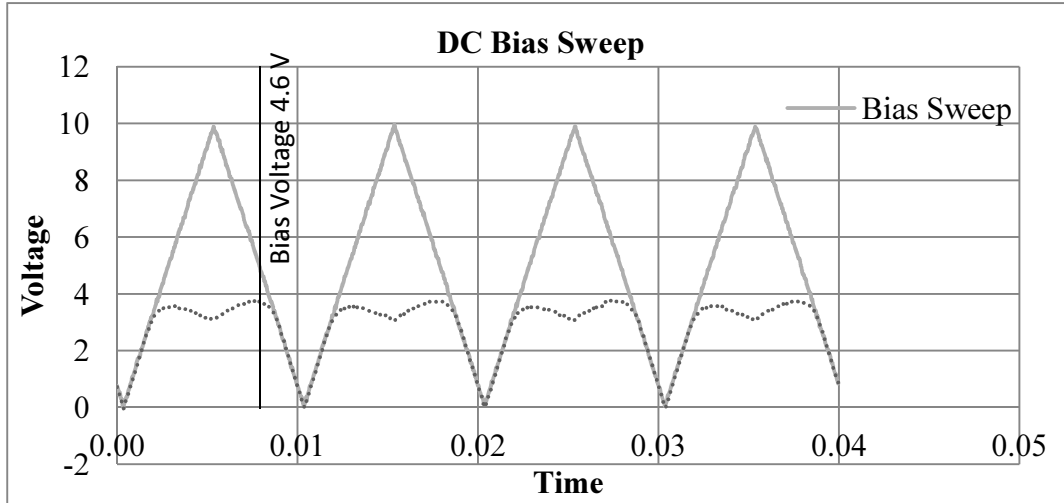
DC Bias Sweep

Fig. 6.3.2 DC bias sweep.

Next, DC offset voltage was measured. The input offset voltage at 25 °C was observed to be 16.9 mV. The offset voltage increased with temperature, observed as 45.7 mV, 48.3 mV and 60 mV at 100 °C, 200 °C and 300 °C, respectively. The offset value, the ICMR and the OVR were measured with Keithley 4200 using the voltage follower configuration. Fig. 6.3.3 shows the variation of offset voltage with temperatures.
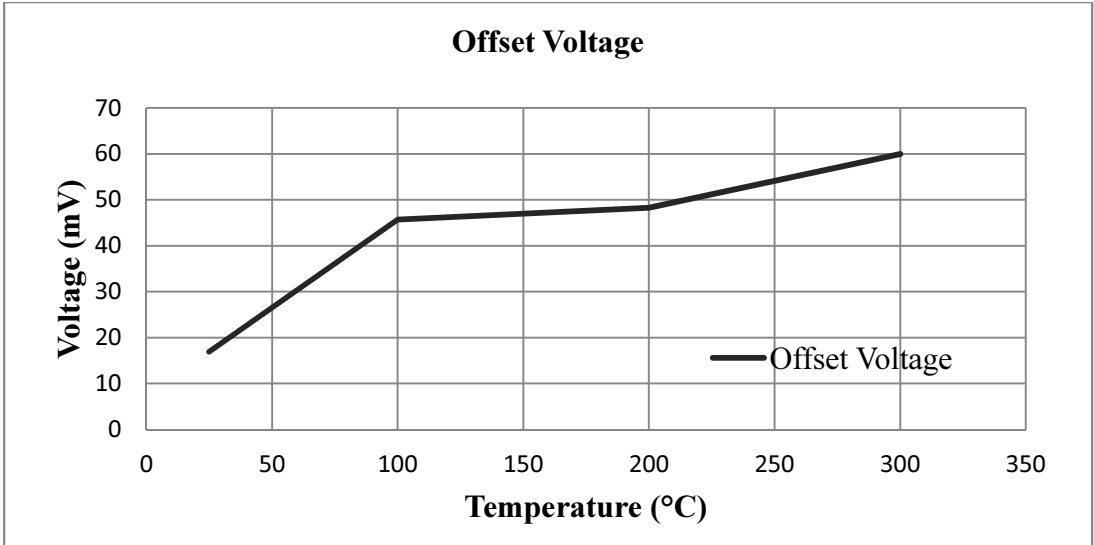
Fig. 6.3.3. The offset voltage at different temperatures

The measured unity-gain mode ICMR, OVR and DC current supply at 25 °C are shown in Fig. 6.3.4.
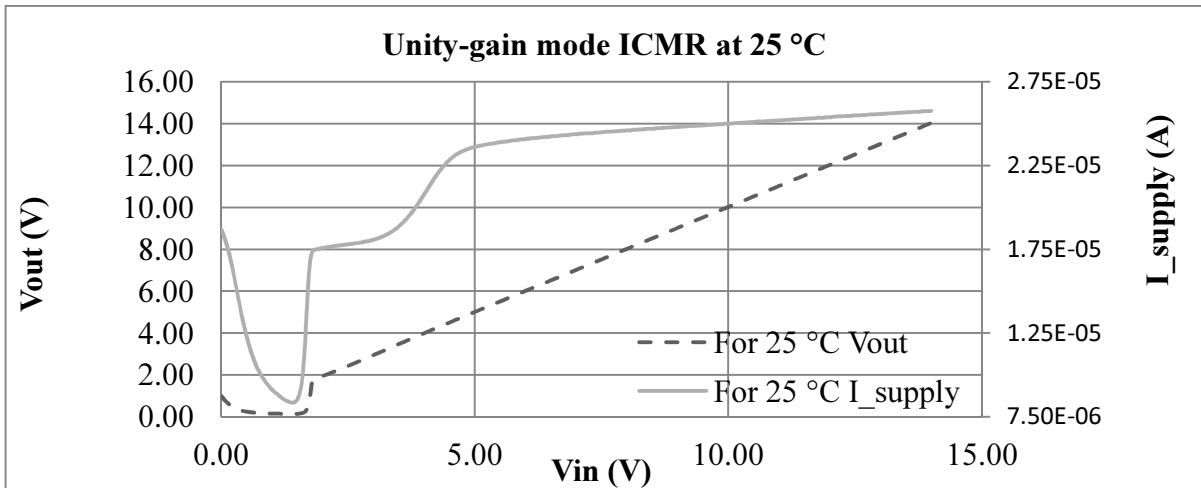
Fig. 6.3.4. Input common mode range at 25 °C.

The measured unity-gain mode ICMR, OVR and DC current supply at 300 °C is shown in Fig. 6.3.5.
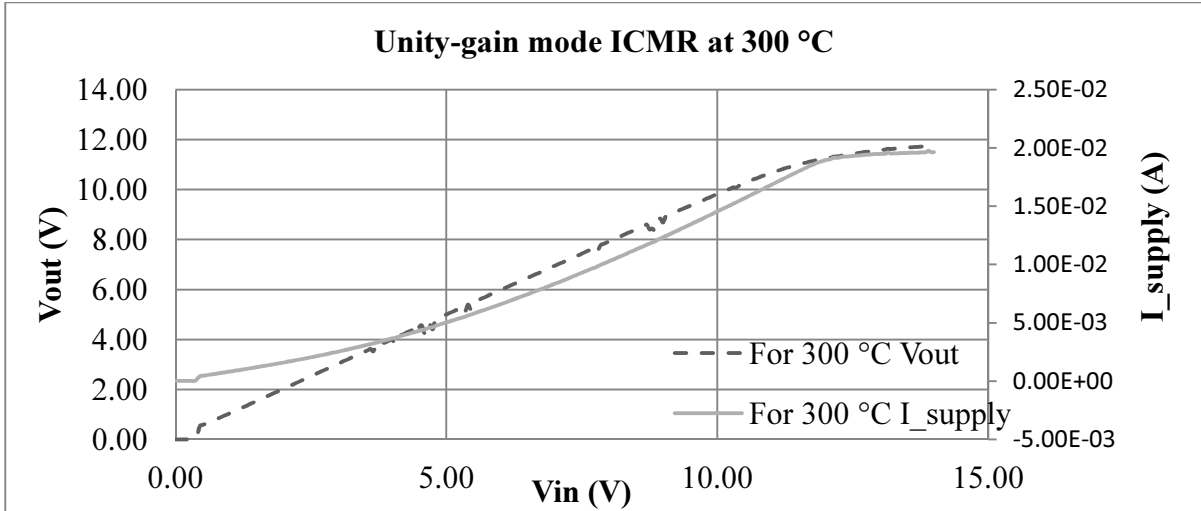
Fig. 6.3.5 Input common mode range at 300 °C.

The unity-gain mode ICMR is 5.85 V to 14.03 V at 25 °C and 5.25 V to 11.8 V at 300 °C. For all temperatures the ICMR range is smaller than simulated values. This is due to the fact that the actual threshold voltages of the transistors are higher than the device model. The OVR is 1.73 V to 14 V at 25 °C and 0.53 V to 11.2 V at 300 °C. The OVR is also smaller than the simulated values due to the same reason. The current consumption and power dissipation at 25 °C is 6.2 mA and 93 mW respectively, and at 300 °C is 18.8 mA and 282 mW respectively. The measured current consumption and power dissipation is higher than simulation due to the fact that a larger bias voltage was required to make sure all of the transistors were in saturation. The summary of the results at different temperature is shown in TABLE 6.3.

56

TABLE 6.3 OP AMP DC CHARACTERISTICS MEASUREMENTS

Parameter	Temperature	Simulated Value	Measured Value	Unit
Offset voltage	25	---	16.9	mV
	100	---	45.7	
	200	---	48.3	
	275/300*	---	60	
Unity-gain ICMR	25	4.7 – 14.58	5.85 – 14.03	V
	100	4.62 – 14.12	5.6 – 13.1	
	200	4.45 – 14.34	5.3 – 12.2	
	275/300*	4.87 – 14.22	5.25 – 11.8	
Output voltage swing range	25	0.69 – 14.45	1.73 – 14	V
	100	0.68 – 14.4	1.37 – 12.8	
	200	0.674 – 14.15	0.53 – 11.6	
	275/300*	0.98 – 14.12	0.53 – 11.2	
Total current consumption	25	0.366	6.2	mA
	100	0.99	11.94	
	200	1.361	15.7	
	275/300*	1.691	18.8	
Power dissipation	25	5.49	93	mW
	100	14.85	179	
	200	20.42	235.5	
	275/300*	25.35	282	

*Simulation/Measurement

Next, transient analysis was performed and a speculation on slew rate and unity-gain bandwidth was measured in Fig. 6.3.6. For the slew rate measurement, a 2 Vp-p (6.5 V to 8.5 V) square wave signal was provided to the positive input of the OTA from the function generator AFG 3022B and the plots were captured by Tecktronix TDS 744A. The specification of the load capacitance in the output was on the order of a few pF (≈10 pF). The output pad was probed using a passive probe. The probe was connected to the oscilloscope through a 4.5 ft RG-174 coaxial cable followed by a 3 ft. RG-58 coaxial cable. The minimum capacitance of the RG-174 is 30.8 pF/ft. [16] and the maximum capacitance of the RG-58 is 26 pF/ft. [17]. So the worst case load capacitance is in the range of 200 pF. The measured slew rate at 25 °C is 13.34 V/μs and at 300 °C is 50 V/μs. The Fig. 6.3.6 shows the slew rate measurement at room temperature.
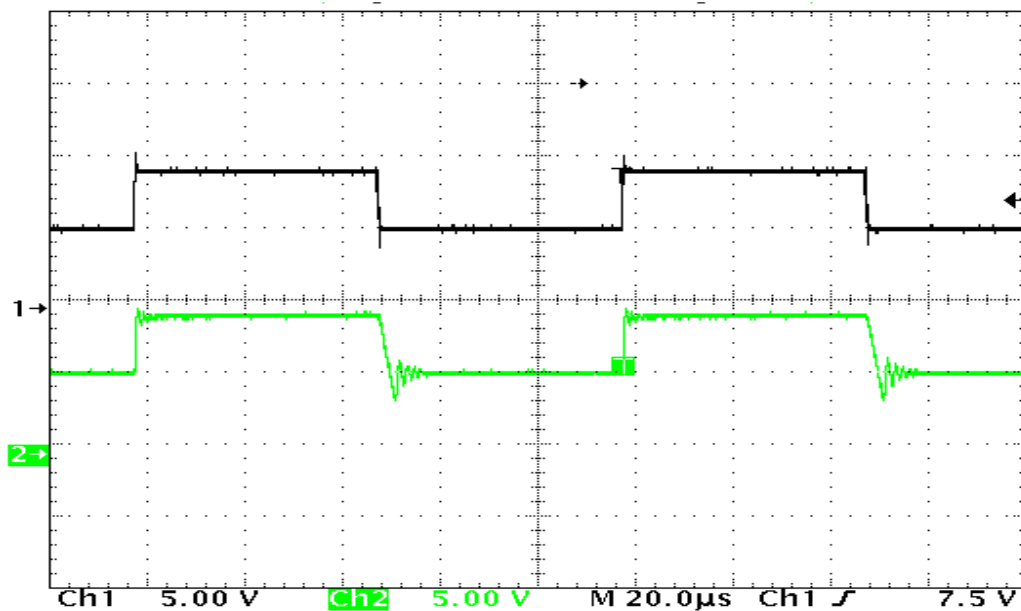
Fig. 6.3.6. Slew rate measurement at 25 °C.

The unity-gain bandwidth with active probe at room temperature is 1.8 MHz and at 300 °C is 6.1 MHz. The used Picoprobe model 12C active probe has 0.1 pF capacitance [18]. The unity-

gain bandwidth with passive probe at room temperature is 1 MHz and at 300 °C is 3.4 MHz. Here with the passive probe at the output, the load is assumed at least 2 times higher than the simulation load. So the unity-gain bandwidth measurements match with the simulation results.

The open loop voltage gain at 25 °C is 63 dB and at 300 °C is 57.5 dB. Although the open loop voltage gain in every temperature is less than the simulation value using BSIM3 model but they match with the simulation value using BSIM4 model. The BSIM4 model has a more accurate frequency response and this model is more closely related with the real output. The Fig. 6.3.7 represents the open loop voltage gain at room temperature.
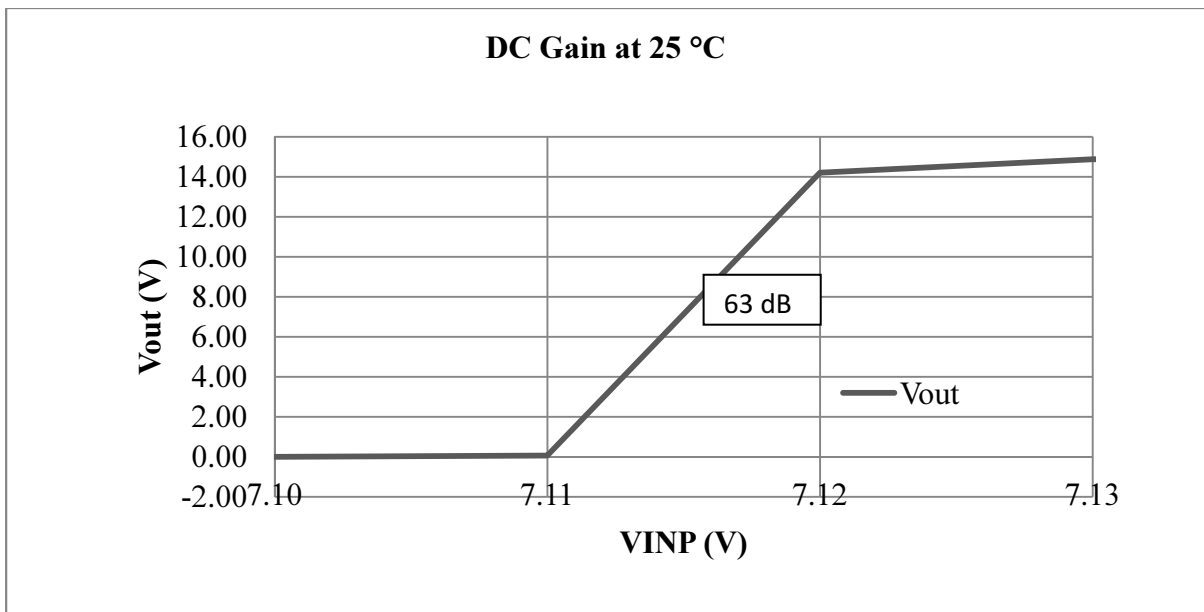
Fig. 6.3.7. DC gain measurement at 25 °C.

The summary of the op amp results at different temperature is shown in TABLE 6.4.

TABLE 6.4 OP AMP AC AND TRANSIENT CHARACTERISTICS MEASUREMENTS

Parameter	Temperature	Simulated Value	Measured Value	Unit
DC gain	25	74.29	63.01	dB
	100	66.32	60	
	200	65.81	58.4	
	275/300[*]	60.84	57.5	
Unity-gain bandwidth	25	2.953	1	MHz
	100	5.895	1.85	
	200	5.985	2.2	
	275/300[*]	6.224	3.4	
Slew rate	25	26.41	13.34	V/μs
	100	71.35	25	
	200	76.6	40	
	275/300[*]	95.88	50	

[*]Simulation/Measurement

CHAPTER 7

CONCLUSION

This thesis has presented the overall design flow of a general purpose two-stage CMOS op amp using SiC CMOS process technology. The designed circuit is one of the pioneering op amp in SiC CMOS technology designed to operate in high temperature range and harsh environment. The purpose of the overall project was to build individual circuit blocks that would be further integrated into a system level design in the next tapeout of NSF-BIC project. An improved version of the designed amplifier has become part of the design of the protection circuitry of a SiC gate driver system that has subsequently been submitted for fabrication.

From the beginning, the main consideration was to design a circuit that would function with good performance characteristics. The pin count has been kept small to simplify testing using both board and probe station methods. This reduced both the time and money required over packaging of random die prior to validation.

The op amp is functional over a wide temperature range and has good performance characteristics. The DC gain of the op amp ranges from 63 dB to 57 dB over temperature (25 °C to 300 °C) and the unity-gain bandwidth ranges from 1 MHz to 3.4 MHz over temperature (25 °C to 300 °C). The op amp shows slew rate from 13.34 V/µs to 50 V/µs over the temperature range. The circuit has high power dissipation: ranging from 93 mW to 282 mW. But for the SiC CMOS process with high threshold voltages ranging from 2.9 V to 5 V with 15 V supply voltage

this power consumption rate is acceptable. The simulations were performed based on BSIM3 models developed for the particular process. The experimental results matches better with the simulation results for the BSIM4 model that developed after the fabrications.

Future Work

Another version of the op amp has been developed and submitted for fabrication in a subsequent run. The simulation of this new three-stage op amp shows good results, but the experimental results still need to confirm functionality. The second version of the op amp needs to be tested using the developed testplan.

REFERENCES

[1] J. Mahattanakul, "Design Procedure for Two-Stage CMOS Opamp With Flexible Noise-Power Balancing Scheme," *CIRCUITS AND SYSTEMS—I: REGULAR PAPERS,* vol. 52, no. 8, pp. 1508-1514, 2005.

[2] A. Vert, Z. Shen and R. Normann, "Silicon Carbide High Temperature Operational Amplifier," in *IMAPS High Temperature Electronics* , Albuquerque, 2012.

[3] A. Francis, A. Rahman, J. Holmes, P. Shepherd, S. Ahmed, M. Barlow, S. Bhuyan, L. Caley, T. Moudy, H. A. Mantooth and J. Di, "Design of Analog and Mixed-Signal Integrated SiC CMOS Circuits with a High Fidelity Process Design Kit," in *Government Microcircuit Applications & Critical Technology Conference*, Charleston , 2014.

[4] B. Razavi, Design of Analog CMOS Integrated Circuits, New York: McGraw-Hill, 2001.

[5] A. Sedra and K. Smith, Microelectronic Circuits Theory and Applications, New Delhi: Oxford University Press, 2009.

[6] D. R. H. Phillip E. Allen, CMOS Analog Circuit Design, 3rd ed., New York: Oxford University Press, Inc., 2012.

[7] W. Jung, "Op Amp Applications Handbook," Newnes Elsevier , Oxford, 2005.

[8] B. Al-Hashimi, J. Fidler and P. Garner, "High Frequency Active Filters using OTAs," in *Electronic Filters, IEE Colloquium*, London, 1989.

[9] R. J. Baker, CMOS Circuit Design, Layout, and Simulation, New Jersey: John Wiley & Sons, Inc. , 2010.

[10] Y. Zhen, "Current Sensing Circuit Concepts and Fundamentals," Microchip Technology Inc., 2010-2011.

[11] R. Thompson, D. Clark, A. Murphy, A. Ramsay, D. Smith, R. Young, J. Cormack, J. McGonigal, J. Fletcher, C. Zhu, S. Finney, L. Martin and A. Horsfall, "High Temperature Silicon Carbide CMS Integrated Circuits," in *International Microelectronics Assembly and Packaging Society* , Oxford, 2011.

[12] F. Amroso, A. Pugliese and G. Cappuccino, "Design Considerations for Fast Settling Two-Stage Miller-Compensated Operational Amplifiers," in *Electronics, Circuits, and Systems*, 2009.

[13] J. Jung, A. Huang and Z. Du, "Simulated Performance of SiC Based OP-AMP at High Temperature," in *Power Electronics Specialists Conference*, 2006.

[14] A. Gupta, D. Mishra, R. Khatri, U. Chandrawat and P. Jain, "A Two Stage and Three Stage CMOS OPAMP with Fast Settling, High DC Gain and Low Power Designed in 180nm Technology," in *Computer Information Systems and Industrial Management Applications* , 2010.

[15] A. Hastings, The Art of Analog Layout, New Jersey: Prentice Hall, 2001.

[16] General Cable, *Product data sheet for part number C1156 (RG 174/U type coaxial cable),* 2011.

[17] West Penn Wire, *Technical data sheet for RG58 coaxial 50 Ohm cable (Part Number 813),* 2010.

[18] GGB Industries Inc., *Picoprobe Model 12C.*

APPENDIX – A

OP AMP TEST PLAN

A. General Power-up Procedure

1. Start with connecting the AVDD and PVDD_IO to +15 V and AVSS and PVSS_IO to common ground 0V to the PCB.

2. Set VBIAS to the desired +4.45V voltage.

3. Depending on the test, place the VINN and VINP connection in the respective AC or DC voltage.

4. Set the power supplies then press the "output off" button.

5. Recheck carefully every voltage of the pins.

6. Wire the pins of the chip in Rogers board with the PCB.

7. Proceed with the test.

8. Measure the results and record the data.

9. After finishing the testing turn of the input signals followed by the bias voltages and power supplies.

B. High Temperature General Procedure

1.   Continue the general power-up procedure from step 1 to 5.

2.   Attach the Roger board in the high temp settings and place it in the hot plate.

3.   Turn on the hot plate and set the required temperature for individual testing.

4.   Continue on the general power-up steps from 6 to 9.

5.   Cool down the chip to room temperature.

C. DC Characterization

DC Offset

1.   The DC offset measurement test bench is shown in Fig. A.C.1.
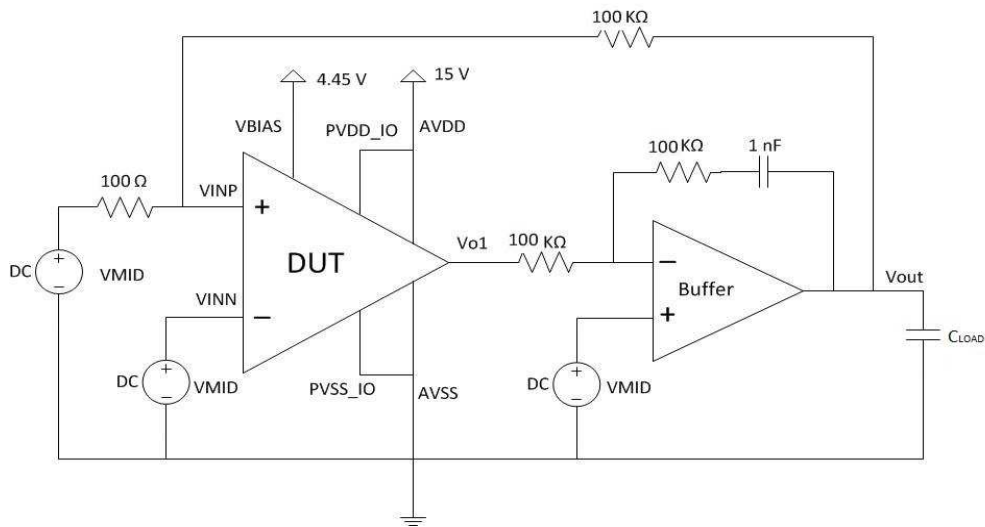
Fig. A.C.1. Input offset voltage measurement

2.   Set up using the general power–up procedure.

3.   Set *VINN* = *VINP* = 7.5 V

4.   Measure Vout using the multimeter.

5.   Determine the relation between the Buffer stage and the Device under test, using the following equation:

$$\Delta Vout = -\Delta Vo1 \qquad\qquad (A.1)$$

6.   The offset voltage V_{OS} can be calculated, using the following equation:

$$V_{offset} \approx \frac{Vout}{1000} \qquad\qquad (A.2)$$
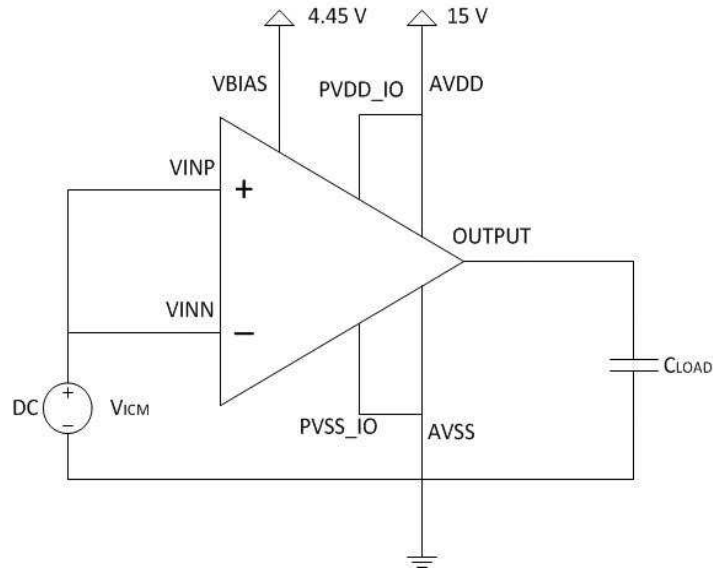
7.   Repeat the test with temperatures ranging from 25 °C to 300°C.

8.   Measure the results and record the offset voltage.

DC Power

1.   Use the test bench as shown in Fig. A.C.1.

2.   Set up using the general power–up procedure.

3.   Set $VINN = VINP = 7.5$ V

4.   Measure the DC current by connecting a multimeter in current mode in series with the power supply. For safety add a 100 Ω resistor between the multimeter and power supply.

5.   Repeat the test with temperatures ranging from 25 °C to 300°C.

6.   Measure the results and record the data.

1.   The ICMR test bench is shown in Fig. A.C.1.

Fig. A.C.2 ICMR measurement circuit

2.   Set up using the general power–up procedure.

3.   DC Sweep V_{CM} from 0 V to 15 V with .5 V step.

4.   Measure the outputs.

5.   Repeat the test with temperatures ranging from 25 ^{o}C to 300°C.

6.   Keep in consideration the offset voltage from the first test and adjust the circuitry to cancel the offset effect.

7.   Repeat the measurement following steps c) to d) for each temperature step.

8.   Measure the results and record the data.

D. AC Characterization

Open Loop Gain

1. The test bench for open loop voltage gain is shown in Fig. A.D.1.
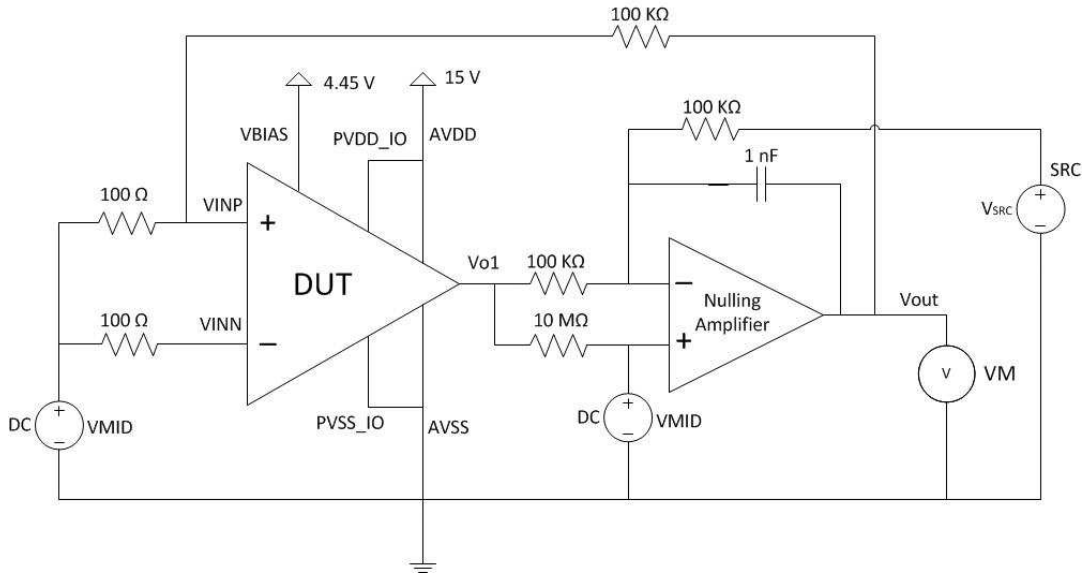
Fig. A.D.1. Open loop gain test bench

2. Set up using the general power–up procedure.

3. Connect VMID to 7.5 V.

4. DC Sweep V_{SRC} from 0V to 15V and measure Vout.

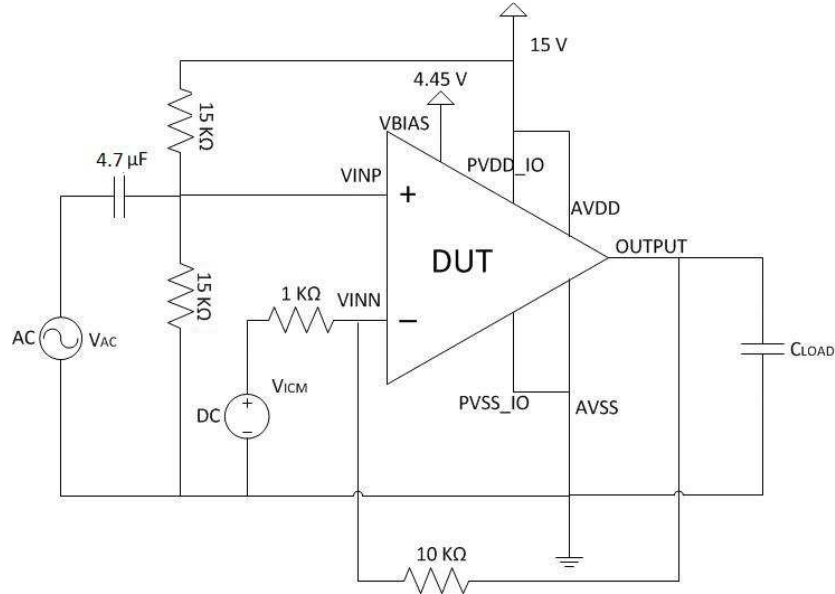5. Calculate the open loop gain using the following equation:

$$Gol = 20\log\left[\frac{100\Omega + 100\ K\Omega}{100\Omega} * \frac{\Delta V_{SRC}}{\Delta Vout}\right] \qquad (A.3)$$

7. Repeat the test with temperatures ranging from 25 ^{o}C to 300 ^{o}C.

6. Measure the results and record the data.

1.   The test bench for unity-gain bandwidth is shown in Fig. A.D.2.
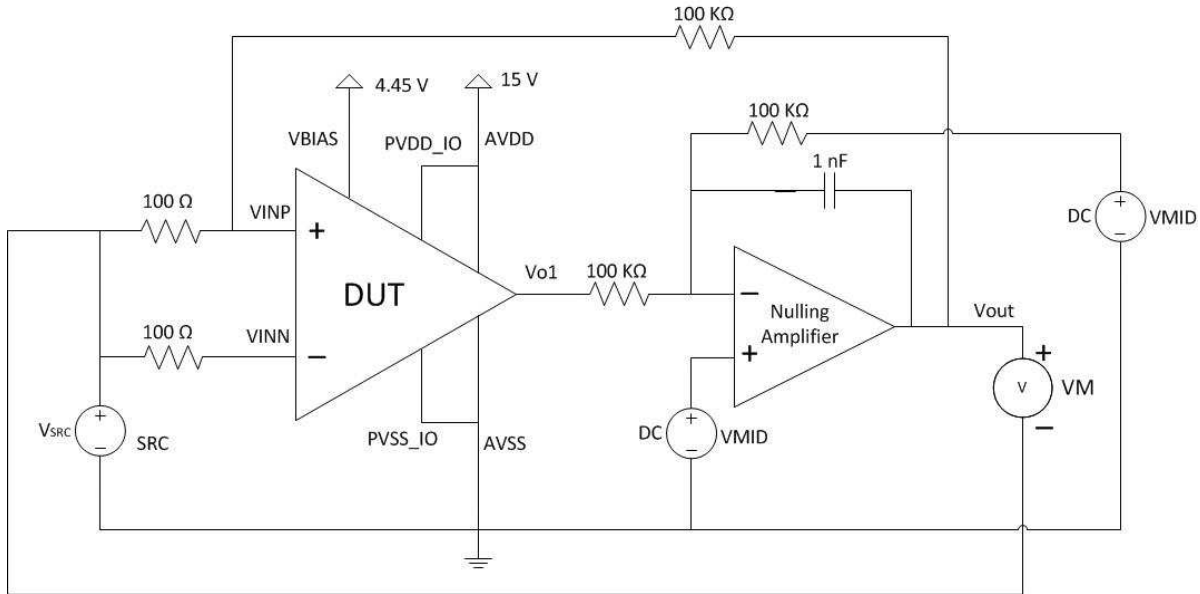

Fig. A.D.2. Test bench for power dissipation and unity gain bandwidth

2.   Set up using the general power–up procedure.

3.   From the arbitrary waveform generator set the sinusoidal input signal. Set the offset

      value, the amplitude to 200 mVp-p, and the frequency to 10 kHz initially.

4.   Connect VINN to 7.5 V.

5.   Sweep the frequency from 1Hz to 10 MHz and measure the frequency for which the

      input is equal to the output i.e. the output signal amplification is zero. This is the

      unity-gain bandwidth.

6.   Repeat the test with temperatures ranging from 25 ^{o}C to 300°C.

7.   Measure the results and record the data.

1.   The test bench for CMRR is shown in Fig.A.D.3.
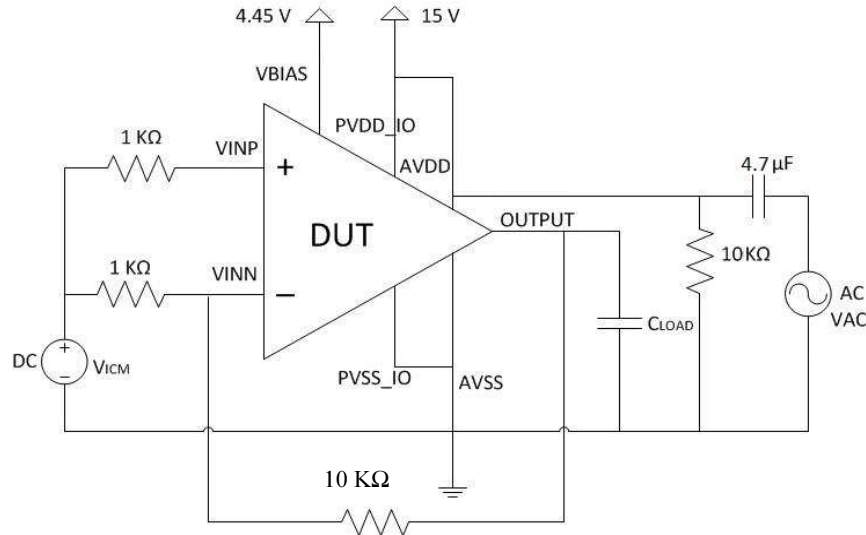

Fig.A.D.3. CMRR test bench

2.   Set up using the general power–up procedure.

3.   Connect VMID to 7.5 V.

4.   Sweep V_{SRC} from 0V to 15V and measure Vout.

5.   Calculate the CMRR using the following equation:

$$CMRR = 20 \log \left[\frac{100\Omega}{100\Omega + 100k\Omega} * \frac{\Delta Vout}{\Delta V_{SRC}} \right] \qquad (A.4)$$

6.   Repeat the test with temperatures ranging from 25 ^{o}C to 300°C.

7.   Measure the results and record the data

Power Supply Rejection Ratio (PSRR)

1. The test bench for PSRR is shown in Fig. A.D.4

Fig. A.D.4. PSRR test bench

2. Set up using the general power–up procedure.

3. From the arbitrary waveform generator set the sinusoidal input signal. Set the offset value, the amplitude to 200 mVp-p, and the frequency to 10 kHz initially.

4. Connect VINN to 7.5 V.

5. Sweep the frequency from 1Hz to 10MHz and measure the differential output.

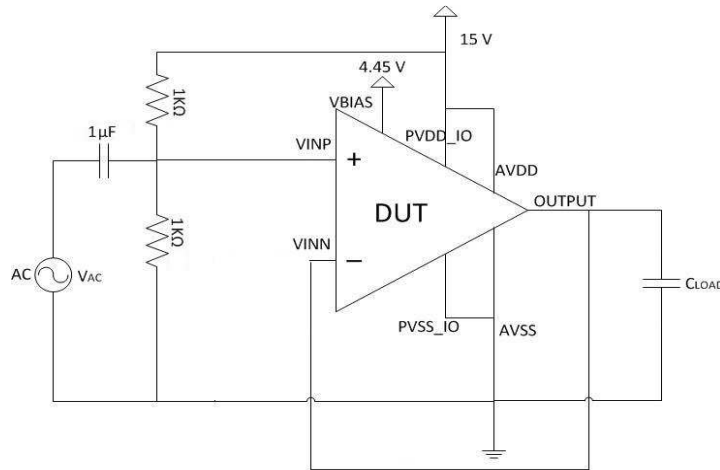6. Calculate the PSRR using the following equation:

$$PSRR = 20 \log \left(\frac{VAC}{Vout} \; X \; 10 \right) \qquad (A.5)$$

7. Repeat the test with temperatures ranging from 25 $^{\circ}$C to 300°C.

8. Measure the results and record the data.

E. Transient Characterization

Slew Rate

1. The test bench for slew rate is shown in Fig. A.E.1

**Fig. A.E.1. Slew rate test bench**

2. Set up using the general power–up procedure.

3. From the arbitrary waveform generator set the input square signal. Set the offset value, the amplitude to 2 Vp-p, and the frequency to 10 kHz initially.

4. Connect VINN to 7.5 V.

5. Calculate the slope of the rising and falling edge. This is the value of the slew rate.

6. Repeat the test with temperatures ranging from 25 $^{\circ}$C to 300°C.

7. Measure the results and record the data.

APPENDIX – B

DESIGN OF AN OP AMP IN THE SUBSEQUENT RUN

The designed and tested op amp has been re-designed in the next fabrication run. The op amp in the run 1 shows instability in the updated BSIM4 model. In this model the circuit performance such as the gain and the phase margin declined: by 9% to 19% for open loop gain and 36% to 38% for phase margin. The range of the phase margin is from 28° to 21°. For this the op amp was unstable. Also special consideration was required for the voltage source bias input. The circuit could be over biased or under biased for a fixed DC bias voltage in different temperatures. Also the threshold voltage of the transistors will also shift due to the voltage biasing.

A more stable op amp with current bias input has been designed in the next run. The schematic of the circuit is shown in the Fig. B.1 below.
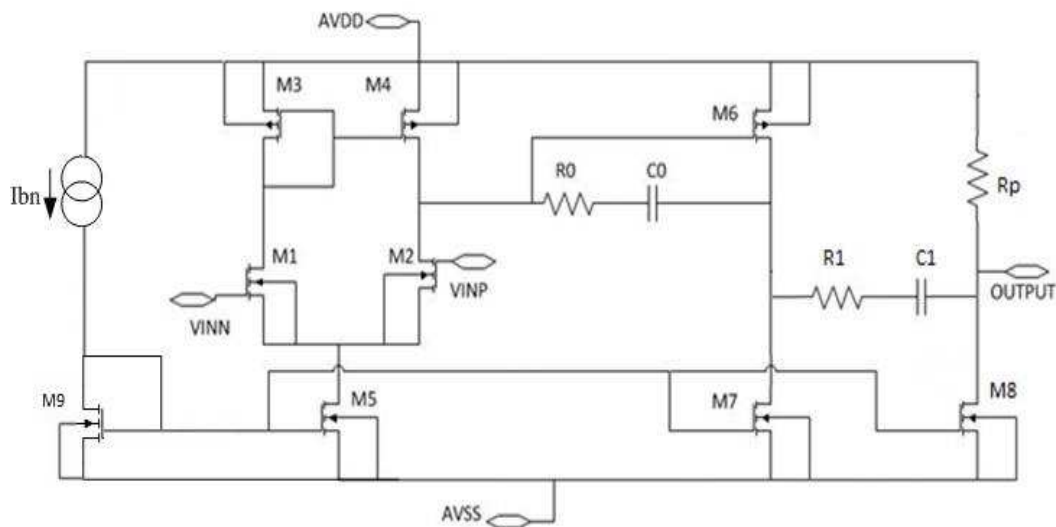
Fig. B.1. Three stage op amp schematics.

This op amp has an added third stage. The third stage is a common source amplifier employed to increase the gain. The increased gain has been traded for the better phase margin. The third stage will introduce more poles and for this another compensation circuit has been added in the op amp. This compensation circuit also consists of a Miller compensation capacitor connected in series with a nulling resistor. The phase margin of the op amp has been improved with the cost of the gain.